Chapter 3
Interpolation of Non-smooth Functions and Anisotropic Polytopal Meshes

The solutions of boundary value problems may contain singularities and/or have layers, where the solution changes rapidly. For such non-smooth functions, the application of pointwise interpolation is not well defined and in the presence of layers the use of regular and uniform meshes is not optimal in some sense. For these reasons quasi-interpolation operators for non-smooth functions over polytopal meshes are introduced and analysed in this chapter. In particular, operators of Clément- and Scott–Zhang-type are studied. Furthermore, the notion of anisotropic meshes is introduced. These meshes do not satisfy the classical regularity properties used in the approximation theory and thus they have to be treated in a special way. However, such meshes allow the accurate and efficient approximation of functions featuring anisotropic behaviours near boundary or interior layers.

3.1 Preliminaries

In the theory of classical interpolation it is assumed that the interpolant is at least in the Sobolev space $H^2(\Omega)$ or even smoother, such that point evaluations are well defined. When talking about non-smooth functions, we have those in mind which are only in $H^1(\Omega)$ and do not satisfy any further regularity. Such functions can be solutions of boundary value problems according to existence and uniqueness theory, cf. the Lax–Milgram Lemma given in Theorem 1.6. But, these functions do not fall in the theory of Sect. 2.5 yielding optimal rates of convergence on sequences of uniformly refined meshes. Instead of using pointwise values for the interpolation of non-smooth functions, one has to exploit averages of the function over certain neighbourhoods of the nodes.

S. Weißer, *BEM-based Finite Element Approaches on Polytopal Meshes*,
Lecture Notes in Computational Science and Engineering 130,
https://doi.org/10.1007/978-3-030-20961-2_3

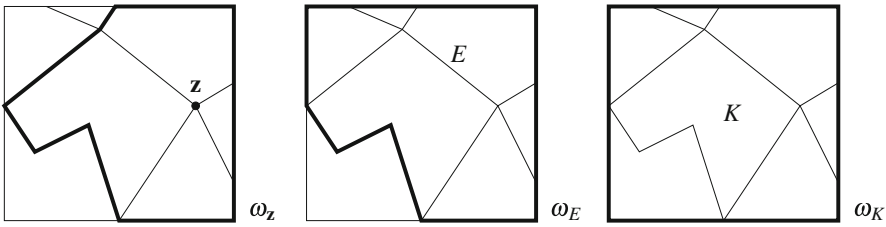

Fig. 3.1 Example of the neighbourhoods of nodes, edges and elements in two space dimensions

Let $\mathscr{K}_h$ be a polytopal mesh of a bounded domain Ω. For each node $\mathbf{z} \in \mathscr{N}_h$ in the mesh we consider its neighbourhood $\omega_{\mathbf{z}}$ defined by

$$\overline{\omega}_{\mathbf{z}} = \bigcup_{\mathbf{z} \in \mathscr{N}(K)} \overline{K}\,, \tag{3.1}$$

where $\mathscr{N}(K)$ denotes the set of all nodes belonging to the element $K \in \mathscr{K}_h$. Furthermore, we introduce the neighbourhoods of edges, faces and elements as

$$\overline{\omega}_E = \bigcup_{\mathbf{z} \in \mathscr{N}(E)} \overline{\omega}_{\mathbf{z}}\,, \qquad \overline{\omega}_F = \bigcup_{\mathbf{z} \in \mathscr{N}(F)} \overline{\omega}_{\mathbf{z}}\,, \qquad \overline{\omega}_K = \bigcup_{\mathbf{z} \in \mathscr{N}(K)} \overline{\omega}_{\mathbf{z}}\,, \tag{3.2}$$

cf. Fig. 3.1 for a visualization in two space dimensions. The neighbourhoods are open sets which are constructed by agglomerating elements next to the corresponding node, edge, face and element, respectively. The diameter of a neighbourhood ω is denoted by h_ω. An important role plays the neighbourhood $\omega_{\mathbf{z}}$. Its diameter $h_{\omega_{\mathbf{z}}}$ is of comparable size to the diameter of $K \subset \omega_{\mathbf{z}}$ as shown in

Lemma 3.1 *Let $\mathscr{K}_h$ be regular and stable mesh of a two- or three-dimensional domain. The following properties hold:*

1. *Each element is covered by a uniformly bounded number of neighbourhoods of elements, i.e. $|\{K' \in \mathscr{K}_h : K \subset \omega_{K'}\}| \le c, \quad \forall K \in \mathscr{K}_h$.*
2. *For all $\mathbf{z} \in \mathscr{N}_h$ and $K \subset \omega_{\mathbf{z}}$, it is $h_{\omega_{\mathbf{z}}} \le c h_K$.*

The constants $c > 0$ only depend on $\sigma_{\mathscr{K}}$, $\sigma_{\mathscr{F}}$ and $c_{\mathscr{K}}$.

Proof The first statement is seen easily. Let $K \in \mathscr{K}_h$ be fixed. Due to the above constructions, the number of element neighbourhoods $\omega_{K'}$ with $K \subset \omega_{K'}$ is equal to the number of elements contained in the neighbourhood ω_K. Consequently, the statement follows since

$$\overline{\omega}_K = \bigcup_{\mathbf{z} \in \mathscr{N}(K)} \overline{\omega}_{\mathbf{z}} = \bigcup_{\mathbf{z} \in \mathscr{N}(K)} \bigcup_{\mathbf{z} \in \mathscr{N}(K')} \overline{K'}\,,$$

and the number of nodes per element as well as the number of elements containing a node are bounded uniformly, see Lemmata 2.7 and 2.16 as well as Corollaries 2.6 and 2.15 for $d = 2$ and $d = 3$, respectively.

In order to see the second statement, we first recognize that

$$h_{\omega_{\mathbf{z}}} \leq 2 \max_{K' \subset \omega_{\mathbf{z}}} h_{K'} \ .$$

Let the maximum be reached for some K'. If K and K' share a common edge E, the stability of the mesh, i.e. $h_{K'} \leq c_{\mathscr{K}} h_E \leq c_{\mathscr{K}} h_K$, gives the desired estimate, namely $h_{\omega_{\mathbf{z}}} \leq 2c_{\mathscr{K}} h_K$. If K and K' do not share a common edge, we can construct a sequence of elements $K_i \subset \omega_{\mathbf{z}}$, $i = 1, \ldots, n$ such that $K_1 = K'$, $K_n = K$ and K_i and K_{i+1} share a common edge. Arguing as above yields

$$h_{\omega_{\mathbf{z}}} \leq 2 \, (c_{\mathscr{K}})^{n-1} \, h_K \ .$$

Since the number of elements contained in $\omega_{\mathbf{z}}$, and thus in particular n, is uniformly bounded according to Corollaries 2.6 and 2.15, the statement is proven. □

In the forthcoming sections, we treat the two- and three-dimensional cases with $d = 2, 3$ simultaneously. Therefore, if we write F, $\mathscr{F}_h$ and so forth, we mean the faces of the discretization for $d = 3$ and with some abuse of notation the edges for $d = 2$. In this chapter, we restrict ourselves to the first order approximation space V_h^1 with $k = 1$ and we simply write V_h for shorter notation. In the three-dimensional case we may use the simple generalization for the construction of V_h introduced in Sect. 2.3.4 which relies on polyhedral elements with triangular faces. The theory in this chapter is also valid for the case of polyhedral elements with polygonal faces. The detailed description of the approximation space is discussed in the later Sect. 6.2. At this point, however, we give a small outlook in order to present the full theory for quasi-interpolation operators. The generalization of V_h to polyhedral elements with polygonal faces reads

$$V_h = \left\{ v \in H^1(\Omega) : \Delta v\big|_K = 0 \ \forall K \in \mathscr{K}_h \text{ and } v\big|_F \in V_h(F) \ \forall F \in \mathscr{F}_h \right\} \ , \tag{3.3}$$

where $V_h(F)$ denotes the two-dimensional discretization space over the face F. The nodal basis functions are constructed as in the two-dimensional case but they have to satisfy additionally the Laplace equation in the linear parameter space of each face.

3.2 Trace Inequality and Best Approximation

Before we introduce quasi-interpolation operators and study error estimates, some analytic auxiliary results are reviewed and extended. These include in particular trace inequalities and approximation results for the L_2-projection into the space of constants over patches of elements. If no confusion arises, we write v for both the function and the trace of the function on an edge and face, respectively.

In the two-dimensional setting, Lemma 2.4 guaranties the existence of the isosceles triangles with common angles for non-convex elements in a regular polygonal mesh. This is sufficient to guaranty the following lemma proven in [174].

Lemma 3.2 *Let $\mathscr{K}_h$ be a regular mesh, $v \in H^1(K)$ for $K \in \mathscr{K}_h$ and $E \in \mathscr{E}(K)$. It holds*

$$\|v\|_{L_2(E)} \leq c \left\{ h_E^{-1/2} \|v\|_{L_2(T_E^{\mathrm{iso}})} + h_E^{1/2} |v|_{H^1(T_E^{\mathrm{iso}})} \right\}$$

with the isosceles triangle $T_E^{\mathrm{iso}} \subset K$ from Lemma 2.4, where c only depends on $\alpha_{\mathscr{K}}$, and thus, on the regularity parameter $\sigma_{\mathscr{K}}$.

Under the additional assumption on the stability of the mesh, we can generalize this trace inequality and state a similar result, which is valid for $d = 2, 3$. Remember the convention that F denotes a face or edge depending on the considered dimensions d.

Lemma 3.3 (Trace Inequality) *Let $\mathscr{K}_h$ be a regular and stable mesh, $v \in H^1(K)$ for $K \in \mathscr{K}_h$ and $F \in \mathscr{F}(K)$. It holds*

$$\|v\|_{L_2(F)} \leq c \left(h_F^{-1/2} \|v\|_{L_2(K)} + h_F^{1/2} |v|_{H^1(K)} \right) ,$$

where c only depends on $\sigma_{\mathscr{K}}$, $\sigma_{\mathscr{F}}$ and $c_{\mathscr{K}}$.

Proof Since $\mathscr{K}_h$ is regular and stable, we have an auxiliary discretization $\mathscr{T}_h(K)$ into tetrahedra such that each face $F \in \mathscr{F}(K)$ is decomposed into triangular facets of these tetrahedra. According to Lemma 2.14 the discretization $\mathscr{T}_h(K)$ is shape regular in the sense of Ciarlet. It is well known, see [2, 40], that there is a constant C only depending on the regularity parameters of the auxiliary discretization such that for $T_{\mathrm{tet}} \in \mathscr{T}_h(K)$ and $v \in H^1(T_{\mathrm{tet}})$ it holds

$$\|v\|^2_{L_2(\partial T_{\mathrm{tet}})} \leq C \left(h_{T_{\mathrm{tet}}}^{-1} \|v\|^2_{L_2(T_{\mathrm{tet}})} + h_{T_{\mathrm{tet}}} \|v\|^2_{H^1(T_{\mathrm{tet}})} \right) .$$

Furthermore, it is $h_F / c_{\mathscr{K}} \leq h_{T_{\mathrm{tet}}} \leq c_{\mathscr{K}} h_F$, cf. Sect. 2.2.2, and thus we obtain for the triangle $T \subset \partial T_{\mathrm{tet}} \cap F$ and $v \in H^1(K)$ that

$$\|v\|^2_{L_2(T)} \leq c \left(h_F^{-1} \|v\|^2_{L_2(T_{\mathrm{tet}})} + h_F \|v\|^2_{H^1(T_{\mathrm{tet}})} \right) .$$

Summing this inequality for all triangles which lie in F yields the desired result. □

Another important analytical tool is the approximation of functions in Sobolev spaces by polynomials. We already applied such results over polytopal elements in the proof of Theorem 2.27. Since these elements are star-shaped, the well known results from [40, 69] are applicable. Next, we consider the polynomial approximation over the neighbourhoods defined in (3.1) and (3.2) which are not star-shaped in general, and therefore we have to extend the theory.

Lemma 3.4 *Let $\mathscr{K}_h$ be a regular and stable mesh and $k \in \mathbb{N}_0$. There exists for every function $v \in H^{k+1}(\omega)$ and every neighbourhood $\omega \in \{\omega_{\mathbf{z}}, \omega_F, \omega_K\}$ a polynomial $p \in \mathscr{P}^k(\omega)$ such that*

$$|v - p|_{H^\ell(\omega)} \leq C\, h_\omega^{k+1-\ell}\, |v|_{H^{k+1}(\omega)} \quad \text{for } \ell = 0, \ldots, k+1 \,,$$

where C only depends on $\sigma_{\mathscr{K}}$, $\sigma_{\mathscr{F}}$ and $c_{\mathscr{K}}$ as well as on k and the dimension d.

Proof Let $\omega \in \{\omega_{\mathbf{z}}, \omega_F, \omega_K\}$, since $\mathscr{K}_h$ is regular and stable, there is an auxiliary discretization of ω into tetrahedra formed by $\mathscr{T}_h(K)$ of all $K \subset \omega$. This discretization is shape regular in the sense of Ciarlet and the number of tetrahedra is uniformly bounded because there are only finitely many K with $K \subset \omega$ according to Lemma 3.1 and each element is decomposed into a bounded number of tetrahedra according to the Lemmata 2.7 and 2.16. Now, that we have a uniformly bounded number of tetrahedra with uniformly bounded aspect ratios due to the regularity, we can argue as in [8] adapting an iterative procedure already mentioned in [69]. We skip the rest of the proof and refer the interested reader to the cited literature. □

The previous result can be applied to obtain error estimates for the L_2-projection. We only consider the projection into the space of constants. For $v \in H^1(\omega)$ this projection is given by

$$\Pi_\omega v = \frac{1}{|\omega|} \int_\omega v(\mathbf{x})\, \mathrm{d}\mathbf{x} \,.$$

It is known that the Poincaré constant

$$C_P(\omega) = \sup_{v \in H^1(\omega)} \frac{\|v - \Pi_\omega v\|_{L_2(\omega)}}{h_\omega |v|_{H^1(\omega)}} < \infty \tag{3.4}$$

is finite and depends on the shape of ω, see [169]. Exploiting that

$$\|v - \Pi_\omega v\|_{L_2(\omega)} = \min_{q \in \mathbb{R}} \|v - q\|_{L_2(\omega)} \,,$$

we deduce from Lemma 3.4 that the Poincaré constant $C_P(\omega)$ is bounded uniformly for the neighbourhoods $\omega \in \{\omega_{\mathbf{z}}, \omega_F, \omega_K\}$ in a regular and stable mesh.

Lemma 3.5 *Let $\mathscr{K}_h$ be a regular and stable mesh. There exists a uniform constant c, which only depends on $\sigma_{\mathscr{K}}$, $\sigma_{\mathscr{F}}$ and $c_{\mathscr{K}}$, such that for every neighbourhood*

$\omega \in \{\omega_{\mathbf{z}}, \omega_F, \omega_K\}$ *with* $\mathbf{z} \in \mathcal{N}_h$, $F \in \mathcal{F}_h$ *and* $K \in \mathcal{K}_h$, *it holds*

$$\|v - \Pi_\omega v\|_{L_2(\omega)} \leq c h_\omega |v|_{H^1(\omega)} \quad \text{for } v \in H^1(\omega) \, .$$

In the following, we give an alternative proof for the two-dimensional case ($d = 2$) with $\omega = \omega_{\mathbf{z}}$. For convex ω, the authors of [136] showed $C_P(\omega) < 1/\pi$. In our situation, however, $\omega_{\mathbf{z}}$ is a patch of non-convex elements which is itself non-convex in general. We proceed as in [180]. The main tool in the forthcoming proof is Proposition 2.10 (Decomposition) of [169]. As preliminary of this proposition, an admissible decomposition $\{\omega_i\}_{i=1}^n$ of ω with pairwise disjoint domains ω_i and

$$\overline{\omega} = \bigcup_{i=1}^{n} \overline{\omega}_i$$

is needed. Admissible means in this context, that there exist triangles $\{T_i\}_{i=1}^n$ such that $T_i \subset \omega_i$ and for every pair i, j of different indices, there is a sequence $i = k_0, \ldots, k_\ell = j$ of indices such that for every m the triangles $T_{k_{m-1}}$ and T_{k_m} share a complete side. Under these assumptions, the Poincaré constant of ω is bounded by

$$C_P(\omega) \leq \max_{1 \leq i \leq n} \left\{ 8(n-1) \left(1 - \min_{1 \leq j \leq n} \frac{|\omega_j|}{|\omega|} \right) \left(C_P^2(\omega_i) + 2 C_P(\omega_i) \right) \frac{|\omega| \, h_{\omega_i}^2}{|T_i| \, h_\omega^2} \right\}^{1/2} . \tag{3.5}$$

Proof (Lemma 3.5, Alternative for $d = 2$ with $\omega = \omega_{\mathbf{z}}$) Before we prove the estimate, we note that $C_P(K) < c$ for an element K which satisfies the regularity and stability assumptions of Definitions 2.1 and 2.2. This follows by remembering the construction of the auxiliary triangulation $\mathcal{T}_h(K)$. K can be interpreted as patch of triangles corresponding to the point $\mathbf{z}_K$. Thus, we choose $\omega_i = T_i$, $i = 1, \ldots, n$ with $\{T_i\}_{i=1}^n = T_h(K)$ for the admissible decomposition of K. The integer n corresponds to the number of nodes in K and thus it is uniformly bounded according to Lemma 2.7. Furthermore, it is $C_P(\omega_i) < 1/\pi$, $|K| < h_K^2$ and $h_{\omega_i}^2 / |T_i| = h_{T_i}^2 / |T_i| \leq c$, because of the shape-regularity of the auxiliary triangulation proven in Lemma 2.3. Consequently, the application of Proposition 2.10 (Decomposition) from [169] yields $C_P(K) < c$.

Now, we address the estimate for general $\omega_{\mathbf{z}}$ in the lemma. Therefore, we apply once more Proposition 2.10 of [169]. For this reason, we construct a decomposition $\{\omega_i\}_{i=1}^n$ and show that it is admissible by giving explicitly a set of triangles $\{T_i\}_{i=1}^n$ which satisfy the above mentioned properties. Furthermore, the terms in (3.5) are estimated.

To simplify the construction, we first assume that the patch consists of only one element, i.e. $\omega_{\mathbf{z}} = K \in \mathcal{K}_h$, and let $E_1, E_2 \in \mathcal{E}(K)$ with $\mathbf{z} = \overline{E}_1 \cap \overline{E}_2$. We decompose $\omega_{\mathbf{z}}$, or equivalently K, into ω_1 and ω_2 such that $n = 2$. The decomposition is done by splitting K along the polygonal chain through the points $\mathbf{z}$, $\mathbf{z}_K$ and $\mathbf{z}'$, where $\mathbf{z}' \in \mathcal{N}(K)$ is chosen such that the angle $\beta = \angle \mathbf{z} \mathbf{z}_K \mathbf{z}'$ is

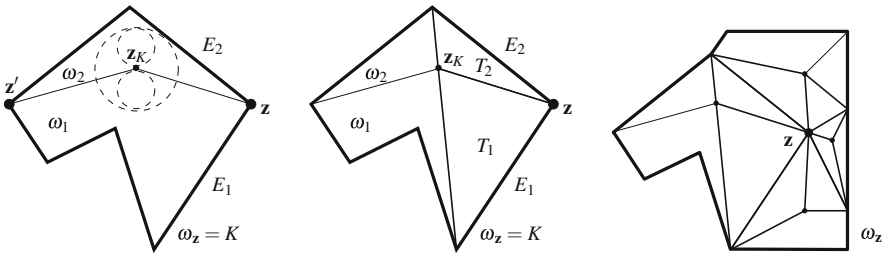

Fig. 3.2 Construction of admissible decomposition for K and $\omega_{\mathbf{z}}$ from Fig. 3.1

maximized, see Fig. 3.2 left. It is $\beta \in (\pi/2, \pi]$, since K is star-shaped with respect to a circle centered at $\mathbf{z}_K$. The triangles $\{T_i\}_{i=1}^n$ are chosen from the auxiliary triangulation in Lemma 2.3 as $T_i = T_{E_i} \in \mathscr{T}_h(K)$, cf. Fig. 3.2 middle. Obviously, $\{\omega_i\}_{i=1}^n$ is an admissible decomposition. Next, we estimate the terms in (3.5) and show that $C_P(\omega_i) \leq c$. The element K is star-shaped with respect to a circle of radius ρ_K and we have split this circle into two circular sectors during the construction of ω_i, $i = 1, 2$. A small calculation shows that ω_i is also star-shaped with respect to a circle of radius

$$\rho_{\omega_i} = \frac{\rho_K \sin(\beta/2)}{1 + \sin(\beta/2)} ,$$

which lies inside the mentioned circular sector and consequently satisfies the relation $\rho_K/(1+\sqrt{2}) < \rho_{\omega_i} \leq \rho_K/2$, see Fig. 3.2 (left). Thus, the aspect ratio of ω_i is uniformly bounded, since

$$\frac{h_{\omega_i}}{\rho_{\omega_i}} \leq \frac{(1+\sqrt{2})h_K}{\rho_K} \leq (1+\sqrt{2})\sigma_{\mathscr{K}} .$$

Furthermore, we observe that $h_{\omega_i} \leq h_K \leq \sigma_{\mathscr{K}} \rho_K \leq \sigma_{\mathscr{K}} |\overline{\mathbf{z}\mathbf{z}_K}|$ and accordingly $h_{\omega_i} \leq \sigma_{\mathscr{K}} |\overline{\mathbf{z}'\mathbf{z}_K}|$. Consequently, ω_i, $i = 1, 2$ is a regular element in the sense of Definition 2.1 and thus, we have already proven that $C_P(\omega_i) \leq c$. Additionally, we obtain by (2.2) and by the regularity of the mesh that

$$\frac{h_{\omega_i}^2}{|T_i|} \leq \frac{2h_{\omega_i}^2}{h_{E_i}\rho_K} \leq \frac{2h_K^2}{h_{E_i}\rho_K} \leq 2c_{\mathscr{K}}\sigma_{\mathscr{K}} .$$

This yields together with $|\omega_{\mathbf{z}}| \leq h_{\omega_{\mathbf{z}}}^2$ and Proposition 2.10 (Decomposition) of [169] that

$$C_P(\omega_{\mathbf{z}}) \leq \left(16(n-1)\left(c^2+2c\right)c_{\mathscr{K}}\sigma_{\mathscr{K}}\right)^{1/2} ,$$

and thus, a uniform bound in the case of $\omega_{\mathbf{z}} = K$ and $n = 2$.

In the general case, the patch $\omega_{\mathbf{z}}$ is a union of several elements, see (3.1) and Fig. 3.1. In this situation, we repeat the construction of ω_i for all neighbouring elements of the node $\mathbf{z}$, see Fig. 3.2 (right). Consequently, n is two times the number of neighbouring elements. This number is uniformly bounded according to Lemma 2.7. The resulting decomposition $\{\omega_i\}_{i=1}^n$ is admissible and the estimate of [169] yields $C_P(\omega_{\mathbf{z}}) \leq c$, where c only depends on $\sigma_{\mathscr{K}}$ and $c_{\mathscr{K}}$. □

Remark 3.6 More precisely, the previous proof yields the estimate

$$C_P(\omega_{\mathbf{z}}) \leq \left(16(n-1)c_{\mathscr{K}}\sigma_{\mathscr{K}} \max_{1\leq i\leq n} \left\{ C_P^2(\omega_i) + 2C_P(\omega_i) \right\} \right)^{1/2},$$

where n is two times the number of elements in $\omega_{\mathbf{z}}$ that is usually a small number. Consequently, $C_P(\omega_{\mathbf{z}})$ is controlled by $C_P(\omega_i)$, $i = 1, \ldots, n$ which only depend on the chunkiness parameter $h_{\omega_i}/\rho_{\omega_i}$ according to [40].

3.3 Quasi-Interpolation of Non-smooth Functions

In the case of smooth functions like in $H^2(\Omega)$, it is possible to use nodal interpolation. Such interpolation operators have been constructed and studied in Sect. 2.4, and they yield optimal approximation error estimates. The goal of this section, however, is to define interpolation for general functions in $H^1(\Omega)$. Consequently, quasi-interpolation operators are applied, which utilizes certain neighbourhoods of the nodes. Classical results on simplicial meshes go back to Clément [59] and to Scott and Zhang [154]. They use L_2-projections instead of point evaluations in order to specify the expansion coefficients in the given basis.

For $v \in H^1(\Omega)$, we are interested in quasi-interpolation operators of the form

$$\mathfrak{I}v = \sum_{\mathbf{z}\in\mathscr{N}_*} (\Pi_{\omega(\psi_{\mathbf{z}})} v)\psi_{\mathbf{z}} \in V_h \,, \tag{3.6}$$

where the set of nodes $\mathscr{N}_*$ and the neighbourhoods $\omega(\psi_{\mathbf{z}})$, which depend on the first order basis functions, have to be specified. The Clément and Scott–Zhang interpolation operators differ in the choice of $\mathscr{N}_*$ and $\omega(\psi_{\mathbf{z}})$. Furthermore, it is desirable that homogeneous Dirichlet data is preserved such that $\mathfrak{I}v \in H_D^1(\Omega)$ for $v \in H_D^1(\Omega)$.

3.3.1 Clément-Type Interpolation

The Clément interpolation operator $\mathfrak{I}_C$ is defined as usual by (3.6), where we choose $\mathscr{N}_* = \mathscr{N}_h \setminus \mathscr{N}_{h,D}$ as all nodes which do not lie on the Dirichlet boundary, and

$\omega(\psi_{\mathbf{z}}) = \omega_{\mathbf{z}}$ as neighbourhood of the nodes. Thus, the interpolation is given as a linear combination of the basis functions $\psi_{\mathbf{z}}$ associated to the nodes in the interior of Ω and the Neumann boundary Γ_N. The expansion coefficients are chosen as average over the neighbourhood of the corresponding nodes. For $v \in H^1_D(\Omega)$, it is $\mathfrak{I}_C v \in H^1_D(\Omega)$ by construction.

Theorem 3.7 *Let $\mathscr{K}_h$ be a regular and stable mesh and let $F \in \mathscr{F}_h$ and $K \in \mathscr{K}_h$. The Clément interpolation operator satisfies for $v \in H^1_D(\Omega)$ the interpolation error estimates*

$$\|v - \mathfrak{I}_C v\|_{L_2(K)} \leq c h_K |v|_{H^1(\omega_K)} \quad \textit{and} \quad \|v - \mathfrak{I}_C v\|_{L_2(F)} \leq c h_F^{1/2} |v|_{H^1(\omega_F)} ,$$

where the constants c only depend on $\sigma_{\mathscr{K}}$, $\sigma_{\mathscr{F}}$ and $c_{\mathscr{K}}$.

Proof The proof follows the arguments of [170, 174] with several modifications for the treatment of polytopal meshes. We start with the first estimate. For $K \in \mathscr{K}_h$, we have the partition of unity property, i.e. $\sum_{\mathbf{z} \in \mathscr{N}(K)} \psi_{\mathbf{z}} = 1$ on $\overline{K}$ and $\|\psi_{\mathbf{z}}\|_{L_\infty(\overline{K})} = 1$ for $\mathbf{z} \in \mathscr{N}(K)$. We distinguish two cases, let all nodes $\mathbf{z} \in \mathscr{N}(K)$ of the element K be located in the interior of Ω or in the interior of the boundary Γ_N, i.e. $\mathbf{z} \in \mathscr{N}_h \setminus \mathscr{N}_{h,D}$. Applying the best approximation result Lemma 3.5, we obtain

$$\begin{aligned}
\|v - \mathfrak{I}_C v\|_{L_2(K)} &\leq \sum_{\mathbf{z} \in \mathscr{N}(K)} \|\psi_{\mathbf{z}} (v - \Pi_{\omega_{\mathbf{z}}} v)\|_{L_2(K)} \\
&\leq \sum_{\mathbf{z} \in \mathscr{N}(K)} \|v - \Pi_{\omega_{\mathbf{z}}} v\|_{L_2(\omega_{\mathbf{z}})} \\
&\leq \sum_{\mathbf{z} \in \mathscr{N}(K)} c h_{\omega_{\mathbf{z}}} |v|_{H^1(\omega_{\mathbf{z}})} \\
&\leq c h_K |v|_{H^1(\omega_K)} .
\end{aligned}$$

In the last step we used that the number of nodes in $\mathscr{N}(K)$ is uniformly bounded, see Lemmata 2.7, 2.16, and 3.1, which gives $h_{\omega_{\mathbf{z}}} \leq c h_K$. In the case that at least one node of the element K is on the Dirichlet boundary Γ_D, i.e. $\mathbf{z} \in \mathscr{N}_{h,D}$, we write

$$\begin{aligned}
v - \mathfrak{I}_C v &= \sum_{\mathbf{z} \in \mathscr{N}(K)} \psi_{\mathbf{z}} v - \sum_{\mathbf{z} \in \mathscr{N}(K) \setminus \mathscr{N}_{h,D}} \psi_{\mathbf{z}} \Pi_{\omega_{\mathbf{z}}} v \\
&= \sum_{\mathbf{z} \in \mathscr{N}(K)} \psi_{\mathbf{z}} (v - \Pi_{\omega_{\mathbf{z}}} v) + \sum_{\mathbf{z} \in \mathscr{N}(K) \cap \mathscr{N}_{h,D}} \psi_{\mathbf{z}} \Pi_{\omega_{\mathbf{z}}} v ,
\end{aligned}$$

and obtain

$$\|v - \mathfrak{I}_C v\|_{L_2(K)} \leq \sum_{\mathbf{z} \in \mathscr{N}(K)} \|\psi_{\mathbf{z}} (v - \Pi_{\omega_{\mathbf{z}}} v)\|_{L_2(K)} + \sum_{\mathbf{z} \in \mathscr{N}(K) \cap \mathscr{N}_{h,D}} \|\psi_{\mathbf{z}} \Pi_{\omega_{\mathbf{z}}} v\|_{L_2(K)} .$$

The first sum has already been treated and the term in the second sum can be estimated by

$$\|\psi_{\mathbf{z}} \Pi_{\omega_{\mathbf{z}}} v\|_{L_2(K)} \leq |\Pi_{\omega_{\mathbf{z}}} v| \, \|\psi_{\mathbf{z}}\|_{L_\infty(K)} \, |K|^{1/2} \leq h_K^{d/2} |\Pi_{\omega_{\mathbf{z}}} v| \, .$$

Because of $\mathbf{z} \in \mathcal{N}_{h,D}$, there is an element $K' \subset \omega_{\mathbf{z}}$ and a face $F' \in \mathcal{F}(K')$ in the Dirichlet boundary, such that $\mathbf{z} \in \mathcal{N}(F')$ and $F' \in \mathcal{F}_{h,D}$. Therefore, v vanishes on F' and we obtain with the trace inequality, see Lemma 3.3,

$$\begin{aligned} |\Pi_{\omega_{\mathbf{z}}} v| &= |F'|^{-1/2} \, \|v - \Pi_{\omega_{\mathbf{z}}} v\|_{L_2(F')} \\ &\leq c |F'|^{-1/2} h_{F'}^{1/2} \left\{ h_{F'}^{-1} \|v - \Pi_{\omega_{\mathbf{z}}} v\|_{L_2(\omega_{\mathbf{z}})} + |v|_{H^1(\omega_{\mathbf{z}})} \right\} \\ &\leq c h_{K'}^{1-d/2} \left\{ h_{\omega_{\mathbf{z}}}^{-1} \|v - \Pi_{\omega_{\mathbf{z}}} v\|_{L_2(\omega_{\mathbf{z}})} + |v|_{H^1(\omega_{\mathbf{z}})} \right\} \, , \end{aligned}$$

where we exploit $h_{K'}^{d-1} \leq c|F'|$, see Remark 2.13, $h_{F'} \leq h_{K'}$, and $h_{\omega_{\mathbf{z}}} \leq c h_{K'} \leq c h_{F'}$ according to Lemma 3.1 and the stability of the mesh. The best approximation, see Lemma 3.5, and the observations $h_K \leq h_{\omega_{\mathbf{z}}} \leq c h_{K'}$ as well as $1 - d/2 \leq 0$ gives

$$|\Pi_{\omega_{\mathbf{z}}} v| \leq c h_K^{1-d/2} |v|_{H^1(\omega_{\mathbf{z}})} \, . \tag{3.7}$$

Putting all estimates together proves the first statement of the theorem.

To prove the second estimate of the theorem, we proceed in a similar manner. Let $F \in \mathcal{F}_h$ be an edge ($d = 2$) or a face ($d = 3$). We have $\sum_{\mathbf{z} \in \mathcal{N}(F)} \psi_{\mathbf{z}} = 1$ on $\overline{F}$ and $\|\psi_{\mathbf{z}}\|_{L_\infty(F)} = 1$ for $\mathbf{z} \in \mathcal{N}(F)$. First, let $F \in \mathcal{F}_h$ be such that all its nodes $\mathbf{z} \in \mathcal{N}(F)$ are located in the interior of Ω or in the interior of the boundary Γ_N, i.e. $\mathbf{z} \in \mathcal{N}_h \setminus \mathcal{N}_{h,D}$. Applying the trace inequality, see Lemma 3.3, with an element $K' \in \mathcal{K}_h$ that satisfies $K' \subset \omega_{\mathbf{z}}$ and $F \in \mathcal{F}(K')$, as well as the best approximation, see Lemma 3.5, we obtain as above

$$\begin{aligned} \|v - \mathfrak{I}_h v\|_{L_2(F)} &\leq \sum_{\mathbf{z} \in \mathcal{N}(F)} \|v - \Pi_{\omega_{\mathbf{z}}} v\|_{L_2(F)} \\ &\leq \sum_{\mathbf{z} \in \mathcal{N}(F)} c h_F^{1/2} \left\{ h_F^{-1} \|v - \Pi_{\omega_{\mathbf{z}}} v\|_{L_2(\omega_{\mathbf{z}})} + |v|_{H^1(\omega_{\mathbf{z}})} \right\} \\ &\leq \sum_{\mathbf{z} \in \mathcal{N}(F)} c h_F^{1/2} |v|_{H^1(\omega_{\mathbf{z}})} \\ &\leq c h_F^{1/2} |v|_{H^1(\omega_F)} \, . \end{aligned}$$

If at least one node of F is on Γ_D, i.e. $\mathbf{z} \in \mathcal{N}_{h,D}$, we have

$$\|v - \mathfrak{I}_h v\|_{L_2(F)} \leq \sum_{\mathbf{z}\in\mathcal{N}(F)} \|\psi_{\mathbf{z}}(v - \Pi_{\omega_{\mathbf{z}}} v)\|_{L_2(F)} + \sum_{\mathbf{z}\in\mathcal{N}(F)\cap\mathcal{N}_{h,D}} \|\psi_{\mathbf{z}}\Pi_{\omega_{\mathbf{z}}} v\|_{L_2(F)} \ .$$

The first sum is treated as before, so let us have a look at the second sum. For $\mathbf{z} \in \mathcal{N}(F) \cap \mathcal{N}_{h,D}$ and some element $K' \in \mathscr{K}_h$ with $F \in \mathscr{F}(K')$, we have according to (3.7)

$$\|\psi_{\mathbf{z}}\Pi_{\omega_{\mathbf{z}}} v\|_{L_2(F)} \leq |F|^{1/2}\,|\Pi_{\omega_{\mathbf{z}}} v| \leq c\,|F|^{1/2}\,h_{K'}^{1-d/2}|v|_{H^1(\omega_{\mathbf{z}})} \leq c\,h_F^{1/2}|v|_{H^1(\omega_{\mathbf{z}})} \ ,$$

where in the last estimate we have used $|F| \leq h_F^{d-1}$ and $h_{K'}^{1-d/2} \leq h_F^{1-d/2}$. Putting all estimates together and exploiting that the number of nodes per edge ($d = 2$) and face ($d = 3$) is uniformly bounded, see Lemma 2.7 and Definition 2.10, yields the second statement of the theorem and concludes the proof. □

3.3.2 Scott–Zhang-Type Interpolation

The Scott–Zhang interpolation operator $\mathfrak{I}_{SZ} : H^1(\Omega) \to V_h$ is defined as usual by (3.6), where we choose $\mathcal{N}_* = \mathcal{N}_h$ and $\omega(\psi_{\mathbf{z}}) = F_{\mathbf{z}}$, where $F_{\mathbf{z}} \in \mathscr{F}_h$ is an edge ($d = 2$) or face ($d = 3$) with $\mathbf{z} \in \overline{F}_{\mathbf{z}}$ and

$$F_{\mathbf{z}} \subset \Gamma_D \text{ if } \mathbf{z} \in \overline{\Gamma}_D \qquad \text{and} \qquad F_{\mathbf{z}} \subset \Omega \cup \Gamma_N \text{ if } \mathbf{z} \in \Omega \cup \Gamma_N \ .$$

Thus, the interpolation is given as a linear combination of all basis functions $\psi_{\mathbf{z}}$. The expansion coefficients are chosen as average over edges and faces. By construction, it is $\mathfrak{I}_{SZ} v \in H_D^1(\Omega)$ for $v \in H_D^1(\Omega)$, such that homogeneous Dirichlet data is preserved. We have the following local stability result, which can be utilized to derive interpolation error estimates.

Lemma 3.8 *Let $\mathscr{K}_h$ be a regular and stable mesh and $K \in \mathscr{K}_h$. The Scott–Zhang interpolation operator satisfies for $v \in H^1(\Omega)$ the local stability*

$$\|\mathfrak{I}_{SZ} v\|_{L_2(K)} \leq c\left(\|v\|_{L_2(\omega_K)} + h_K|v|_{H^1(\omega_K)}\right) \ ,$$

where the constant c only depends on $\sigma_{\mathscr{K}}$, $\sigma_{\mathscr{F}}$ and $c_{\mathscr{K}}$.

Proof The only non-vanishing basis functions $\psi_{\mathbf{z}}$ over K in the expansion of $\mathfrak{I}_{SZ} v$ are those with $\mathbf{z} \in \mathcal{N}(K)$. Due to the stability of the L_2-projection $\Pi_{F_{\mathbf{z}}}$ we have $\|\Pi_{F_{\mathbf{z}}} v\|_{L_2(F_{\mathbf{z}})} \leq \|v\|_{L_2(F_{\mathbf{z}})}$. Furthermore, there exists $K_{\mathbf{z}} \in \mathscr{K}_h$ with $F_{\mathbf{z}} \subset \partial K_{\mathbf{z}}$ such

that $K_{\mathbf{z}} \subset \omega_K$. Therefore, we obtain with the trace inequality, see Lemma 3.3,

$$\begin{aligned}
|\Pi_{F_{\mathbf{z}}} v| &= |F_{\mathbf{z}}|^{-1/2} \, \|\Pi_{F_{\mathbf{z}}} v\|_{L_2(F_{\mathbf{z}})} \\
&\leq c \, |F_{\mathbf{z}}|^{-1/2} h_{F_{\mathbf{z}}}^{-1/2} \left(\|v\|_{L_2(K_{\mathbf{z}})} + h_{F_{\mathbf{z}}} |v|_{H^1(K_{\mathbf{z}})} \right) \\
&\leq c \, |K_{\mathbf{z}}|^{-1/2} \left(\|v\|_{L_2(K_{\mathbf{z}})} + h_{K_{\mathbf{z}}} |v|_{H^1(K_{\mathbf{z}})} \right) \, ,
\end{aligned}$$

since $|K_{\mathbf{z}}| \leq h_{K_{\mathbf{z}}}^d \leq c_{\mathscr{K}}^d h_{F_{\mathbf{z}}}^{d-1} h_{F_{\mathbf{z}}} \leq c |F_{\mathbf{z}}| h_{F_{\mathbf{z}}}$ and $h_{F_{\mathbf{z}}} \leq h_{K_{\mathbf{z}}}$ due to the regularity and stability of the mesh. Utilizing this estimate and $\|\psi_{\mathbf{z}}\|_{L_\infty(K)} = 1$ yields

$$\begin{aligned}
\|\mathfrak{I}_{SZ} v\|_{L_2(K)} &\leq \sum_{\mathbf{z} \in \mathscr{N}(K)} \|(\Pi_{F_{\mathbf{z}}} v) \, \psi_{\mathbf{z}}\|_{L_2(K)} \\
&\leq \sum_{\mathbf{z} \in \mathscr{N}(K)} |(\Pi_{F_{\mathbf{z}}} v)| \, \|\psi_{\mathbf{z}}\|_{L_\infty(K)} \, |K|^{1/2} \\
&\leq c \sum_{\mathbf{z} \in \mathscr{N}(K)} \left(\frac{|K|}{|K_{\mathbf{z}}|} \right)^{1/2} \left(\|v\|_{L_2(K_{\mathbf{z}})} + h_{K_{\mathbf{z}}} |v|_{H^1(K_{\mathbf{z}})} \right) \, .
\end{aligned}$$

Furthermore, it is $K, K_{\mathbf{z}} \subset \omega_{\mathbf{z}}$ and thus $h_{K_{\mathbf{z}}} \leq h_{\omega_{\mathbf{z}}}$. Lemma 3.1 yields $h_{\omega_{\mathbf{z}}} \leq c h_K$ and consequently $h_{K_{\mathbf{z}}} \leq c h_K$. Additionally, we can bound $|K|/|K_{\mathbf{z}}|$ uniformly, because of $|K| \leq h_K^d \leq c h_{K_{\mathbf{z}}}^d \leq c \sigma_{\mathscr{K}}^d \rho_{K_{\mathbf{z}}}^d \leq c |K_{\mathbf{z}}|$, since the d-dimensional ball of radius $\rho_{K_{\mathbf{z}}}$ is inscribed in $K_{\mathbf{z}}$. Exploiting that $K_{\mathbf{z}} \subset \omega_K$ and that the number of nodes per element is uniformly bounded, see Lemmata 2.7 and 2.16, finishes the proof. □

Theorem 3.9 *Let $\mathscr{K}_h$ be a regular and stable mesh and $K \in \mathscr{K}_h$. The Scott–Zhang interpolation operator satisfies for $v \in H^1(\Omega)$ the interpolation error estimate*

$$\|v - \mathfrak{I}_{SZ} v\|_{L_2(K)} \leq c h_K |v|_{H^1(\omega_K)} \, ,$$

where the constant c only depends on $\sigma_{\mathscr{K}}$, $\sigma_{\mathscr{F}}$ and $c_{\mathscr{K}}$.

Proof For $p = \Pi_{\omega_K} v \in \mathbb{R}$ it is obviously $p = \mathfrak{I}_{SZ} p$ and $\nabla p = 0$. The estimate in the theorem follows by Lemma 3.8 and the application of Lemma 3.4, since

$$\begin{aligned}
\|v - \mathfrak{I}_{SZ} v\|_{L_2(K)} &\leq \|v - p\|_{L_2(K)} + \|\mathfrak{I}_{SZ}(v - p)\|_{L_2(K)} \\
&\leq c \left(\|v - p\|_{L_2(\omega_K)} + h_K |v|_{H^1(\omega_K)} \right) \\
&\leq c h_K |v|_{H^1(\omega_K)} \, .
\end{aligned}$$

□

3.4 Anisotropic Polytopal Meshes

When dealing with highly anisotropic solutions of boundary value problems, it is widely recognized that anisotropic mesh refinements have significant potential for improving the efficiency of the solution process. Pioneering works for the analysis of finite element methods on anisotropic meshes have been performed by Apel [10] as well as by Formaggia and Perotto [78, 79]. The meshes usually consist of triangular and quadrilateral elements in two-dimension as well as on tetrahedral and hexahedral elements in three-dimension. First results on a posteriori error estimates for driving adaptive mesh refinement with anisotropic elements have been derived by Kunert [119] for triangular and tetrahedral meshes. For the mesh generation and adaptation different concepts are available which rely on metric-based strategies, see, e.g., [108, 125], or on splitting of elements, see [152] and the references therein. The anisotropic splitting of classical elements, however, results in certain restrictions why several authors combine this approach with additional strategies like edge swapping, node removal and local node movement. These restrictions come from the limited element shapes and the necessity to remove or handle hanging nodes in the discretization. For three-dimensional elements the situation is even more difficult. In contrast, anisotropic polytopal elements promise a high potential in the accurate resolution of sharp layers in the solutions of boundary value problems due to their enormous flexibility. An appropriate framework is developed in this section.

3.4.1 Characterisation of Anisotropy and Regularity

Let $K \subset \mathbb{R}^d$, $d = 2, 3$ be a bounded polytopal element. Furthermore, we assume that K is not degenerated, i.e. $|K| = \text{meas}_d(K) > 0$. We define the center or mean of K as

$$\bar{\mathbf{x}}_K = \frac{1}{|K|} \int_K \mathbf{x} \, \mathrm{d}\mathbf{x}$$

and the covariance matrix of K as

$$M_{\text{Cov}}(K) = \frac{1}{|K|} \int_K (\mathbf{x} - \bar{\mathbf{x}}_K)(\mathbf{x} - \bar{\mathbf{x}}_K)^\top \, \mathrm{d}\mathbf{x} \in \mathbb{R}^{d \times d} \, .$$

This matrix has already been used in Sect. 2.2.3 for the bisection of elements in the discussion of mesh refinement. Obviously, M_{Cov} is real valued, symmetric and positive definite since K is not degenerated. Therefore, it admits an eigenvalue decomposition

$$M_{\text{Cov}}(K) = U_K \Lambda_K U_K^\top$$

with

$$U_K^\top = U_K^{-1} \quad \text{and} \quad \Lambda_K = \operatorname{diag}(\lambda_{K,1}, \ldots, \lambda_{K,d}) \, .$$

Without loss of generality, let the eigenvalues satisfy $\lambda_{K,1} \geq \ldots \geq \lambda_{K,d} > 0$ and we assume that the corresponding eigenvectors $\mathbf{u}_{K,1}, \ldots, \mathbf{u}_{K,d}$, collected in U, form a basis of $\mathbb{R}^d$ with the same orientation for all considered elements $K \in \mathscr{K}_h$.

The eigenvectors of $M_{\mathrm{Cov}}(K)$ give the characteristic directions of K. This fact is, e.g., also used in the principal component analysis (PCA). The eigenvalue $\lambda_{K,j}$ is the variance of the underlying data in the direction of the corresponding eigenvector $\mathbf{u}_{K,j}$. Thus, the square root of the eigenvalues give the standard deviations in a statistical setting. Consequently, if

$$M_{\mathrm{Cov}}(K) = cI$$

for $c > 0$, there are no dominant directions in the element K. We characterise the anisotropy with the help of the quotient $\lambda_{K,1}/\lambda_{K,d} \geq 1$ and call an element

$$\text{isotropic, if} \quad \frac{\lambda_{K,1}}{\lambda_{K,d}} \approx 1 \, ,$$

$$\text{and anisotropic, if} \quad \frac{\lambda_{K,1}}{\lambda_{K,d}} \gg 1 \, .$$

For $d = 3$, we might even characterise whether the element is anisotropic in one or more directions by comparing the different combinations of eigenvalues.

Exploiting the spectral information of the polytopal elements, we next introduce a linear transformation of an anisotropic element K onto a kind of reference element $\widehat{K}$. For each $\mathbf{x} \in K$, we define the mapping by

$$\mathbf{x} \mapsto \widehat{\mathbf{x}} = \mathfrak{F}_K(\mathbf{x}) = A_K \mathbf{x} \quad \text{with} \quad A_K = \alpha_K \Lambda_K^{-1/2} U_K^\top \, , \tag{3.8}$$

and $\alpha_K > 0$, which will be chosen later. $\widehat{K} = \mathfrak{F}_K(K)$ is called reference configuration later on.

Lemma 3.10 *Under the above transformation, it holds*

1. $|\widehat{K}| = |K| \, |\det(A_K)| = \alpha_K^d |K| / \sqrt{\prod_{j=1}^d \lambda_{K,j}}$,
2. $\bar{\mathbf{x}}_{\widehat{K}} = \mathfrak{F}_K(\bar{\mathbf{x}}_K)$,
3. $M_{\mathrm{Cov}}(\widehat{K}) = \alpha_K^2 I$.

Proof First, we recognize that

$$\det(A_K) = \alpha_K^d \det(\Lambda_K^{-1/2} U_K^\top) = \alpha_K^d / \sqrt{\det(\Lambda_K)} = \alpha_K^d / \sqrt{\prod_{j=1}^d \lambda_{K,j}} \, .$$

Consequently, we obtain by the transformation

$$|\widehat{K}| = \int_{\widehat{K}} \mathrm{d}\widehat{\mathbf{x}} = |K|\,|\det(A_K)| = \alpha_K^d |K| / \sqrt{\det(M_{\mathrm{Cov}}(K))}\ ,$$

that proves the first statement. For the center, we have

$$\bar{\mathbf{x}}_{\widehat{K}} = \frac{1}{|\widehat{K}|} \int_{\widehat{K}} \widehat{\mathbf{x}}\, \mathrm{d}\widehat{\mathbf{x}} = \frac{|\det(A_K)|}{|\widehat{K}|} A_K \int_K \mathbf{x}\, \mathrm{d}\mathbf{x} = A_K \bar{\mathbf{x}}_K = \mathfrak{F}_K(\bar{\mathbf{x}}_K)\ .$$

The covariance matrix has the form

$$\begin{aligned} M_{\mathrm{Cov}}(\widehat{K}) &= \frac{1}{|\widehat{K}|} \int_{\widehat{K}} (\widehat{\mathbf{x}} - \bar{\mathbf{x}}_{\widehat{K}})(\widehat{\mathbf{x}} - \bar{\mathbf{x}}_{\widehat{K}})^\top \, \mathrm{d}\widehat{\mathbf{x}} \\ &= \frac{|\det(A_K)|}{|\widehat{K}|} \int_K A_K(\mathbf{x} - \bar{\mathbf{x}}_K)\,(A_K(\mathbf{x} - \bar{\mathbf{x}}_K))^\top \, \mathrm{d}\mathbf{x} \\ &= A_K M_{\mathrm{Cov}}(K) A_K^\top \\ &= \alpha_K^2 (\Lambda_K^{-1/2} U_K^\top)(U_K \Lambda_K U_K^\top)(\Lambda_K^{-1/2} U_K^\top)^\top \\ &= \alpha_K^2\, I\ , \end{aligned}$$

that finishes the proof. □

According to the previous lemma, the reference configuration $\widehat{K}$ is isotropic, since $\lambda_{\widehat{K},1}/\lambda_{\widehat{K},d} = 1$, and thus, it has no dominant direction. We can still choose the parameter α_K in the mapping. We might use $\alpha_K = 1$ such that the variance of the element in every direction is equal to one. On the other hand, we can use the parameter α_K in order to normalise the volume of $\widehat{K}$ such that $|\widehat{K}| = 1$. This is achieved by

$$\alpha_K = \left(\frac{\sqrt{\det(M_{\mathrm{Cov}}(K))}}{|K|} \right)^{1/d} = \left(\frac{\sqrt{\prod_{j=1}^d \lambda_{K,j}}}{|K|} \right)^{1/d}\ , \tag{3.9}$$

see Lemma 3.10, and will be used in the following.

Example 3.11 The transformation (3.8) for α_K according to (3.9) is demonstrated for an anisotropic element $K \subset \mathbb{R}^2$, i.e. $d = 2$. The element K is depicted in Fig. 3.3 (left). The eigenvalues of $M_{\mathrm{Cov}}(K)$ are

$$\lambda_{K,1} \approx 111.46 \quad \text{and} \quad \lambda_{K,2} \approx 1.18\ ,$$

and thus

$$\frac{\lambda_{K,1}}{\lambda_{K,2}} \approx 94.40 \gg 1\ .$$

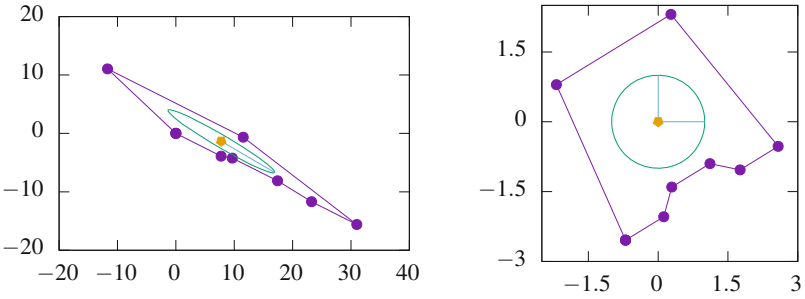

Fig. 3.3 Demonstration of transformation (3.8): original anisotropic element (left) and transformed element centered at the origin (right)

In Fig. 3.3, we additionally visualize the eigenvectors of $M_{\mathrm{Cov}}(K)$ scaled by the square root of their corresponding eigenvalue and centered at the mean of the element. The ellipse is the one given uniquely by the scaled vectors. In the right picture of Fig. 3.3, the transformed element $\widehat{K} = \mathfrak{F}_K(K)$ is given with the scaled eigenvectors of its covariant matrix $M_{\mathrm{Cov}}(\widehat{K})$. The computation verifies $|\widehat{K}| = 1$, and we have

$$M_{\mathrm{Cov}}(\widehat{K}) \approx \begin{pmatrix} 8.59 \cdot 10^{-2} & -3.93 \cdot 10^{-17} \\ -3.93 \cdot 10^{-17} & 8.59 \cdot 10^{-2} \end{pmatrix} .$$

In view of the quasi-interpolation and interpolation operators and their approximation properties, the meshes have to guaranty certain requirements. In the previous analysis of such operators, we made use of isotropic polytopal elements in regular and stable meshes $\mathscr{K}_h$. The corresponding definitions of Sect. 2.2 are summarized in the following remark.

Remark 3.12 Let $\mathscr{K}_h$ be a polytopal mesh. $\mathscr{K}_h$ is called a regular and stable (isotropic) mesh, if all elements $K \in \mathscr{K}_h$ satisfy:

1. K is a star-shaped polygon/polyhedron with respect to a circle/ball of radius ρ_K and midpoint $\mathbf{z}_K$.
2. The aspect ratio is uniformly bounded from above by $\sigma_{\mathscr{K}}$, i.e. $h_K/\rho_K < \sigma_{\mathscr{K}}$.
3. For the element K and all its edges $E \in \mathscr{E}(K)$ it holds $h_K \leq c_{\mathscr{K}} h_E$.
4. In the case $d = 3$, all polygonal faces $F \in \mathscr{F}(K)$ of the polyhedral element K are star-shaped with respect to a circle of radius ρ_F and midpoint $\mathbf{z}_F$ and their aspect ratio is uniformly bounded, i.e. $h_F/\rho_F < \sigma_{\mathscr{F}}$.

Obviously, these assumptions are not satisfied in the case of anisotropic meshes. The aspect ratio of the element depicted in Fig. 3.3 (left) is very large and one of its edges degenerates compared with the element diameter. In the definition of regular and stable anisotropic meshes, we make use of the previously introduced reference configuration.

Definition 3.13 (Regular and Stable Anisotropic Mesh) Let $\mathscr{K}_h$ be a polytopal mesh. $\mathscr{K}_h$ is called a regular and stable anisotropic mesh, if:

1. The reference configuration $\widehat{K}$ for all $K \in \mathscr{K}_h$ obtained by (3.8) is a regular and stable polytopal element according to Sect. 2.2, see Remark 3.12.
2. Neighbouring elements behave similarly in their anisotropy. More precisely, for two neighbouring elements K_1 and K_2, i.e. $\overline{K}_1 \cap \overline{K}_2 \neq \varnothing$, with covariance matrices

$$M_{\mathrm{Cov}}(K_1) = U_{K_1} \Lambda_{K_1} U_{K_1}^\top \quad \text{and} \quad M_{\mathrm{Cov}}(K_2) = U_{K_2} \Lambda_{K_2} U_{K_2}^\top$$

as defined above, we can write

$$\Lambda_{K_2} = (I + \Delta^{K_1,K_2}) \Lambda_{K_1} \quad \text{and} \quad U_{K_2} = R^{K_1,K_2} U_{K_1}$$

with

$$\Delta^{K_1,K_2} = \mathrm{diag}\left(\delta_j^{K_1,K_2} : j = 1, \dots, d\right) ,$$

and a rotation matrix $R^{K_1,K_2} \in \mathbb{R}^{d\times d}$ such that for $j = 1, \dots, d$

$$0 \leq |\delta_j^{K_1,K_2}| < c_\delta < 1 \quad \text{and} \quad 0 \leq \|R^{K_1,K_2} - I\|_2 \left(\frac{\lambda_{K_1,1}}{\lambda_{K_1,d}}\right)^{1/2} < c_R$$

uniformly for all neighbouring elements, where $\|\cdot\|_2$ denotes the spectral norm.

In the rest of the chapter, the generic constant c may also depend on c_δ and c_R.

Remark 3.14 For $d = 2$, the rotation matrix has the form

$$R^{K_1,K_2} = \begin{pmatrix} \cos\phi^{K_1,K_2} & -\sin\phi^{K_1,K_2} \\ \sin\phi^{K_1,K_2} & \cos\phi^{K_1,K_2} \end{pmatrix} ,$$

with an angle ϕ^{K_1,K_2}. For the spectral norm $\|R^{K_1,K_2} - I\|_2$, we recognize that

$$(R^{K_1,K_2} - I)^\top (R^{K_1,K_2} - I) = \left(\sin^2\phi^{K_1,K_2} + (1 - \cos\phi^{K_1,K_2})^2\right) I ,$$

and consequently

$$\begin{aligned} \|R^{K_1,K_2} - I\|_2 &= \left(\sin^2\phi^{K_1,K_2} + (1 - \cos\phi^{K_1,K_2})^2\right)^{1/2} \\ &= 2\left|\sin\left(\frac{\phi^{K_1,K_2}}{2}\right) - \sin(0)\right| \\ &\leq |\phi^{K_1,K_2}| , \end{aligned}$$

according to the mean value theorem. The assumption on the spectral norm in Definition 3.13 can thus be replaced by

$$|\phi^{K_1,K_2}| \left(\frac{\lambda_{K_1,1}}{\lambda_{K_1,2}} \right)^{1/2} < c_\phi \ .$$

This implies that neighbouring highly anisotropic elements have to be aligned in almost the same directions, whereas isotropic or moderately anisotropic elements might vary in their characteristic directions locally.

Let us study the reference configuration $\widehat{K} \subset \mathbb{R}^d$, $d = 2, 3$ of $K \in \mathscr{K}_h$, which is regular and stable. Due to the scaling with α_K, it is $|\widehat{K}| = 1$ and we obtain

$$1 = |\widehat{K}| \le h_{\widehat{K}}^d \le \sigma_{\mathscr{K}}^d \rho_{\widehat{K}}^d = \sigma_{\mathscr{K}}^d \ \nu\pi\rho_{\widehat{K}}^d \ / \ (\nu\pi) \le \sigma_{\mathscr{K}}^d \ |\widehat{K}| \ / \ (\nu\pi) = \sigma_{\mathscr{K}}^d \ / \ (\nu\pi) \ ,$$

where $\nu = 1$ for $d = 2$ and $\nu = 4/3$ for $d = 3$, since the circle/ball is inscribed the element $\widehat{K}$. Consequently, we obtain

$$1 \le h_{\widehat{K}} \le \frac{\sigma_{\mathscr{K}}}{(\nu\pi)^{1/d}} \ . \tag{3.10}$$

Furthermore, for $d = 3$, let $\widehat{F}$ be a face of $\widehat{K}$ and denote by $\widehat{E}$ one of its edges, i.e., $\widehat{E} \in \mathscr{E}(\widehat{F})$. Due to the regularity and stability, we find

$$|\widehat{F}| \ge \pi\rho_{\widehat{F}}^2 \ge \pi h_{\widehat{F}}^2/\sigma_{\mathscr{F}}^2 \ge \pi h_{\widehat{E}}^2/\sigma_{\mathscr{F}}^2 \ge \pi h_{\widehat{K}}^2/(c_{\mathscr{K}}\sigma_{\mathscr{F}}^2) \ ,$$

and thus for $d = 2, 3$

$$h_{\widehat{K}}^{d-1} \le c|\widehat{F}| \ . \tag{3.11}$$

A regular and stable anisotropic element can be mapped according to the previous definition onto a regular and stable polytopal element in the usual sense. In the definition of quasi-interpolation operators, we deal, however, with patches of elements instead of single elements. Thus, we have to study the mapping of such patches. These include in particular the patches $\omega_{\mathbf{z}}$, ω_F and ω_K defined in Sect. 3.1.

Lemma 3.15 *Let $\mathscr{K}_h$ be a regular and stable anisotropic mesh, $\omega_{\mathbf{z}}$ be the patch of elements corresponding to the node $\mathbf{z} \in \mathscr{N}_h$, and $K_1, K_2 \in \mathscr{K}_h$ with $K_1, K_2 \subset \omega_{\mathbf{z}}$. The mapped element $\mathfrak{F}_{K_1}(K_2)$ is regular and stable in the sense of Sect. 2.2, see Remark 3.12, with slightly perturbed regularity and stability parameters $\widetilde{\sigma}_{\mathscr{K}}$ and $\widetilde{c}_{\mathscr{K}}$ depending only on the regularity and stability of $\mathscr{K}_h$. Consequently, the mapped patch $\mathfrak{F}_K(\omega_{\mathbf{z}})$ consists of regular and stable polytopal elements for all $K \in \mathscr{K}_h$ with $K \subset \omega_{\mathbf{z}}$.*

Proof We verify Remark 3.12 for the mapped element $\widetilde{K}_2 = \mathfrak{F}_{K_1}(K_2)$.

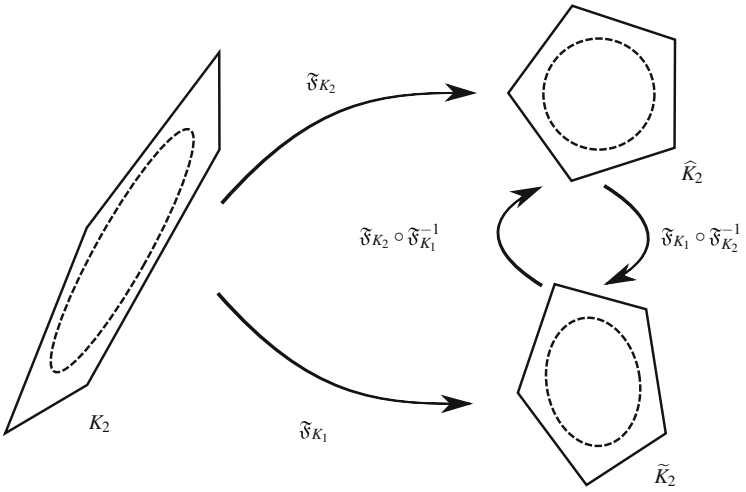

Fig. 3.4 Anisotropic element K_2 with mapped regular and stable element $\widehat{K}_2$ (reference configuration) and perturbed mapped element $\widetilde{K}_2 = \mathfrak{F}_{K_1}(K_2)$

First, we address 1. of Remark 3.12. $\widehat{K}_2 = \mathfrak{F}_{K_2}(K_2)$ is regular and thus, star-shaped with respect to a circle/ball $\widehat{B}$. If we transform $\widehat{K}_2$ into $\widetilde{K}_2$ with the mapping $\mathfrak{F}_{K_1} \circ \mathfrak{F}_{K_2}^{-1}$, see Fig. 3.4, the circle/ball $\widehat{B}$ is transformed into an ellipse/ellipsoid $\widetilde{B} = \mathfrak{F}_{K_1} \circ \mathfrak{F}_{K_2}^{-1}(\widehat{B})$. Since the transformations are linear, the element $\widetilde{K}_2$ is star-shaped with respect to the ellipse/ellipsoid $\widetilde{B}$ and in particular with respect to the circle/ball inscribed $\widetilde{B}$.

Next, we address 2. of Remark 3.12 and we bound the aspect ratio. The radius $\rho_{\widetilde{K}_2}$ of the inscribed circle/ball as above is equal to the smallest semi-axis of the ellipse/ellipsoid $\widetilde{B}$. Let $\widetilde{\mathbf{x}}_1$ and $\widetilde{\mathbf{x}}_2$ be the intersection of $\widetilde{B}$ and the inscribed circle/ball. Thus, we obtain

$$
\begin{aligned}
2\rho_{\widehat{K}_2} &= |\mathfrak{F}_{K_2} \circ \mathfrak{F}_{K_1}^{-1}(\widetilde{\mathbf{x}}_1 - \widetilde{\mathbf{x}}_2)| \\
&= \left| \alpha_{K_2} \Lambda_{K_2}^{-1/2} U_{K_2}^\top \frac{1}{\alpha_{K_1}} U_{K_1} \Lambda_{K_1}^{1/2} (\widetilde{\mathbf{x}}_1 - \widetilde{\mathbf{x}}_2) \right| \\
&= \frac{\alpha_{K_2}}{\alpha_{K_1}} \left| \Lambda_{K_1}^{-1/2} (I + \Delta^{K_1,K_2})^{-1/2} U_{K_1}^\top \left(R^{K_1,K_2} \right)^\top U_{K_1} \Lambda_{K_1}^{1/2} (\widetilde{\mathbf{x}}_1 - \widetilde{\mathbf{x}}_2) \right| \\
&= \frac{\alpha_{K_2}}{\alpha_{K_1}} \left| (I + \Delta^{K_1,K_2})^{-1/2} \left(\Lambda_{K_1}^{-1/2} U_{K_1}^\top \left(R^{K_1,K_2} - I \right)^\top U_{K_1} \Lambda_{K_1}^{1/2} + I \right) (\widetilde{\mathbf{x}}_1 - \widetilde{\mathbf{x}}_2) \right| \\
&\leq \frac{\alpha_{K_2}}{\alpha_{K_1}} \left\| (I + \Delta^{K_1,K_2})^{-1/2} \right\|_2 \left(\|\Lambda_{K_1}^{-1/2}\|_2 \|R^{K_1,K_2} - I\|_2 \|\Lambda_{K_1}^{1/2}\|_2 + 1 \right) 2\rho_{\widetilde{K}_2} \\
&= \frac{\alpha_{K_2}}{\alpha_{K_1}} \max_{j=1,\dots,d} \left\{ (1 + \delta_j^{K_1,K_2})^{-1/2} \right\} \left(1 + \left(\frac{\lambda_{K_1,1}}{\lambda_{K_1,d}} \right)^{1/2} \|R^{K_1,K_2} - I\|_2 \right) 2\rho_{\widetilde{K}_2} ,
\end{aligned}
$$

since the spectral norm $\|\cdot\|_2$ is invariant under orthogonal transformations and, in particular, under rotations like U_{K_1}. With similar arguments, we can bound $h_{\widetilde{K}_2}$. Therefore, let $\widetilde{\mathbf{x}}_1, \widetilde{\mathbf{x}}_2 \in \partial\widetilde{K}_2$ be such that $h_{\widetilde{K}_2} = |\widetilde{\mathbf{x}}_1 - \widetilde{\mathbf{x}}_2|$ and $\widehat{\mathbf{x}}_i = \mathfrak{F}_{K_2} \circ \mathfrak{F}_{K_1}^{-1}(\widetilde{\mathbf{x}}_i) \in \partial\widehat{K}_2$, $i = 1, 2$. With similar considerations as above, we obtain

$$
\begin{aligned}
h_{\widetilde{K}_2} &= |\mathfrak{F}_{K_1} \circ \mathfrak{F}_{K_2}^{-1}(\widehat{\mathbf{x}}_1 - \widehat{\mathbf{x}}_2)| \\
&\leq \frac{\alpha_{K_1}}{\alpha_{K_2}} \max_{j=1,\dots,d} \left\{ (1 + \delta_j^{K_1,K_2})^{1/2} \right\} \left(1 + \left(\frac{\lambda_{K_1,1}}{\lambda_{K_1,d}} \right)^{1/2} \|R^{K_1,K_2} - I\|_2 \right) h_{\widehat{K}_2} \, .
\end{aligned}
$$

Exploiting the last two estimates yields

$$
\begin{aligned}
\frac{h_{\widetilde{K}_2}}{\rho_{\widetilde{K}_2}} &\leq \frac{\max_{j=1,\dots,d} \sqrt{1 + \delta_j^{K_1,K_2}}}{\min_{j=1,\dots,d} \sqrt{1 + \delta_j^{K_1,K_2}}} \left(1 + \left(\frac{\lambda_{K_1,1}}{\lambda_{K_1,d}} \right)^{1/2} \|R^{K_1,K_2} - I\|_2 \right)^2 \frac{h_{\widehat{K}_2}}{\rho_{\widehat{K}_2}} \\
&\leq \sqrt{\frac{1 + c_\delta}{1 - c_\delta}} \, (1 + c_R)^2 \, \frac{h_{\widehat{K}_2}}{\rho_{\widehat{K}_2}} \leq \sqrt{\frac{1 + c_\delta}{1 - c_\delta}} \, (1 + c_R)^2 \, \sigma_{\mathscr{K}} = \widetilde{\sigma}_{\mathscr{K}} \, .
\end{aligned}
$$

Obviously, the aspect ratio is uniformly bounded from above by a perturbed regularity parameter $\widetilde{\sigma}_{\mathscr{K}}$.

Finally we address 3. of Remark 3.12. Let $\widetilde{E}$ be an edge of $\widetilde{K}_2$ with endpoints $\widetilde{\mathbf{x}}_1$ and $\widetilde{\mathbf{x}}_2$. Furthermore, let $\widehat{E}$ be the corresponding edge of $\widehat{K}_2$ with endpoints $\widehat{\mathbf{x}}_1$ and $\widehat{\mathbf{x}}_2$. In the penultimate equation we estimated $h_{\widetilde{K}_2}$ by a term times $h_{\widehat{K}_2}$. Due to the stability it is $h_{\widehat{K}_2} \leq c_{\mathscr{K}} h_{\widehat{E}}$ and, as in the estimate of $\rho_{\widehat{K}_2}$ above, we find that

$$
\begin{aligned}
h_{\widehat{E}} &= |\widehat{\mathbf{x}}_1 - \widehat{\mathbf{x}}_2| = |\mathfrak{F}_{K_2} \circ \mathfrak{F}_{K_1}^{-1}(\widetilde{\mathbf{x}}_1 - \widetilde{\mathbf{x}}_2)| \\
&\leq \frac{\alpha_{K_2}}{\alpha_{K_1}} \max_{j=1,\dots,d} \left\{ (1 + \delta_j^{K_1,K_2})^{-1/2} \right\} \left(1 + \left(\frac{\lambda_{K_1,1}}{\lambda_{K_1,d}} \right)^{1/2} \|R^{K_1,K_2} - I\|_2 \right) h_{\widetilde{E}} \, .
\end{aligned}
$$

Summarizing, we obtain

$$
h_{\widetilde{K}_2} \leq \sqrt{\frac{1 + c_\delta}{1 - c_\delta}} \, (1 + c_R)^2 \, c_{\mathscr{K}} \, h_{\widetilde{E}} = \widetilde{c}_{\mathscr{K}} h_{\widetilde{E}} \, .
$$

□

Remark 3.16 According to the previous proof, the perturbed regularity and stability parameters are given by

$$
\widetilde{\sigma}_{\mathscr{K}} = \sqrt{\frac{1 + c_\delta}{1 - c_\delta}} \, (1 + c_R)^2 \, \sigma_{\mathscr{K}} \quad \text{and} \quad \widetilde{c}_{\mathscr{K}} = \sqrt{\frac{1 + c_\delta}{1 - c_\delta}} \, (1 + c_R)^2 \, c_{\mathscr{K}} \, .
$$

Proposition 3.17 *Let $K \in \mathscr{K}_h$ be a polytopal element of a regular and stable anisotropic mesh $\mathscr{K}_h$ and $F \in \mathscr{F}_h$ one of its edges ($d = 2$) or faces ($d = 3$). The mapped patches $\mathfrak{F}_K(\omega_K)$ and $\mathfrak{F}_K(\omega_F)$ consist of regular and stable polytopal elements.*

Proof The mapped patches $\mathfrak{F}_K(\omega_{\mathbf{z}})$, $\mathbf{z} \in \mathscr{N}(K)$ consist of regular and stable polytopal elements according to Lemma 3.15. Since ω_K and ω_F are given as union of the neighbourhoods $\omega_{\mathbf{z}}$, see (3.2), the statement of the proposition follows. □

Proposition 3.18 *Each node $\mathbf{z} \in \mathscr{N}_h$ of a regular and stable anisotropic mesh $\mathscr{K}_h$ belongs to a uniformly bounded number of elements and, vice versa, each element $K \in \mathscr{K}_h$ has a uniformly bounded number of nodes on its boundary.*

Proof Let $\omega_{\mathbf{z}}$ be the neighbourhood of the node $\mathbf{z}$. According to Lemma 3.15, the mapped neighbourhood $\widetilde{\omega}_{\mathbf{z}}$ consists of regular and stable polytopal elements, which admit a shape-regular decomposition into simplices (triangles or tetrahedra). The mapped node $\widetilde{\mathbf{z}}$ therefore belongs to a uniformly bounded number of simplices and thus to finitely many polytopal elements, cf. Sect. 2.2. Since $\widetilde{\omega}_{\mathbf{z}}$ is obtained by a linear transformation, we follow that $\mathbf{z}$ belongs to a uniformly bounded number of anisotropic elements. With the same argument we see that $\widetilde{K}$ and thus K has a uniformly bounded number of nodes on its boundary. □

Remark 3.19 In the publications of Apel and Kunert (see e.g. [10, 119]), it is assumed that neighbouring triangles/tetrahedra behave similarly. More precisely, they assume:

- The number of tetrahedra containing a node $\mathbf{z}$ is bounded uniformly.
- The dimension of adjacent tetrahedra must not change rapidly, i.e.

$$h_{i,T} \sim h_{i,T'} \quad \forall T, T' \text{ with } T \cap T' \neq \varnothing,\ i = 1, 2, 3,$$

  where $h_{1,T} \geq h_{2,T} \geq h_{3,T}$ are the heights of the tetrahedron T over its faces.

The first point is always satisfied in our setting according to the previous proposition. The second point corresponds to our assumption that Λ_{K_1} and Λ_{K_2} differ moderately for neighbouring elements K_1 and K_2, see Definition 3.13. The assumption on U_{K_1} and U_{K_2} in the definition ensure that the heights are aligned in the same directions, this is also hidden in the assumption of Apel and Kunert.

The regularity of the mapped patches has several consequences, which are exploited in later proofs.

Lemma 3.20 *Let K_1, K_2 be polytopal elements of a regular and stable anisotropic mesh $\mathscr{K}_h$, $\omega_{\mathbf{z}}$ and ω_{K_1} be the neighbourhoods of the node $\mathbf{z} \in \mathscr{N}_h$ and the element K_1, respectively. Furthermore, let $K_1, K_2 \subset \omega_{\mathbf{z}}$. We have for the mapped patch $\widetilde{\omega} \in \{\mathfrak{F}_{K_1}(\omega_{\mathbf{z}}), \mathfrak{F}_{K_1}(\omega_{K_1})\}$ and the neighbouring elements, that*

$$h_{\widetilde{\omega}} \leq c \qquad \text{and} \qquad \frac{|K_2|}{|K_1|} \leq c\ ,$$

where the constants only depend on the regularity and stability parameters of the mesh.

Proof According to Lemma 3.15 and Proposition 3.17 the patch $\widetilde{\omega}$ consists of regular and stable polytopal elements. Obviously, it is $h_{\widetilde{\omega}} \leq C \max\{h_{\widetilde{K}} : \widetilde{K} \subset \widetilde{\omega}\}$, where the constant takes the value $C = 2$ for $\widetilde{\omega} = \mathfrak{F}_{K_1}(\omega_{\mathbf{z}})$ and $C = 3$ for $\widetilde{\omega} = \mathfrak{F}_{K_1}(\omega_{K_1})$, respectively. Let us assume without loss of generality that the maximum is reached for $\widetilde{K}$ which shares a common edge $\widetilde{E}$ with $\widetilde{K}_1$. Otherwise consider a sequence of polytopal elements in $\widetilde{\omega}$, cf. Lemma 3.1. Due to the regularity and stability of the elements, it is

$$h_{\widetilde{\omega}} \leq 3h_{\widetilde{K}} \leq 3c_{\mathscr{K}} h_{\widetilde{E}} \leq 3c_{\mathscr{K}} h_{\widetilde{K}_1} \leq \frac{3c_{\mathscr{K}}\sigma_{\mathscr{K}}}{(\nu\pi)^{1/d}}$$

according to (3.10), since $\widetilde{K}_1 = \mathfrak{F}_{K_1}(K_1) = \widehat{K}_1$.

In order to prove the second estimate, we observe that $|K_1| = |\widehat{K}_1|/|\det(A_{K_1})|$, see Lemma 3.10. The same variable transform yields $|K_2| = |\widetilde{K}_2|/|\det(A_{K_1})|$, where $\widetilde{K}_2 = \mathfrak{F}_{K_1}(K_2)$. Thus, we obtain

$$\frac{|K_2|}{|K_1|} = \frac{|\widetilde{K}_2|}{|\widehat{K}_1|} = |\widetilde{K}_2| \leq |\widetilde{\omega}_{\mathbf{z}}| \leq h_{\widetilde{\omega}_{\mathbf{z}}}^d \leq c$$

and finish the proof. □

3.4.2 Approximation Space

The approximation space V_h is defined in such a way that the functions $v_h \in V_h$ are harmonic on each element, cf. (3.3). This property originates from the definition of basis functions ψ in Sect. 2.3 as local solutions of Laplace and Poisson problems over the physical elements $K \in \mathscr{K}_h$. In classical finite element methods, however, the basis functions are usually introduced over a reference element. In order to obtain the approximation space over a general physical element these basis functions from the reference element are mapped to the physical one. This strategy has not been addressed so far for polytopal elements due to the lack of an appropriate reference element. But, in the previous section we introduced a reference configuration $\widehat{K}$ for an element K. Thus, we can define basis functions $\widehat{\psi}$ on $\widehat{K}$ as in Sect. 2.3 which are in the lowest order case harmonic and map them onto the physical element K such that $\psi^{\mathrm{ref}} = \widehat{\psi} \circ \mathfrak{F}_K$. In general, these functions are not harmonic anymore on the physical elements, i.e. $\Delta\psi^{\mathrm{ref}} \neq 0$ in K. More precisely, we obtain by the transformation (3.8)

$$\operatorname{div}\left(M_{\mathrm{Cov}}(K)\nabla\psi^{\mathrm{ref}}\right) = 0 \quad \text{in } K \ .$$

Hence, ψ^{ref} is defined to fulfil an anisotropic diffusion equation on K. This is consistent in the sense, that if K is already a reference configuration, i.e. $K = \widehat{K}$, then it is $\Delta\psi^{\text{ref}} = 0$ because of $M_{\text{Cov}}(K) = \alpha_K^2 I$, cf. Lemma 3.10. Thus, nodal basis functions $\psi_{\mathbf{z}}^{\text{ref}}$ constructed this way coincide with the nodal basis function $\psi_{\mathbf{z}}$ defined by (2.6) in Sect. 2.3.1.

The approximation space constructed as described above is denoted by V_h^{ref} since the reference configuration is exploited. For the sake of simplicity we restrict ourselves here to $k = 1$ as well as to the two-dimensional case and to the three-dimensional case with solely triangular faces of the polyhedra. Then, we can also write

$$V_h^{\text{ref}} = \left\{ v \in H^1(\Omega) : \operatorname{div}\left(M_{\text{Cov}}(K)\nabla v\right)\big|_K = 0 \text{ and } v|_{\partial K} \in \mathscr{P}^1_{\text{pw}}(\partial K)\ \forall K \in \mathscr{K}_h \right\} .$$

The spaces V_h and V_h^{ref} share two important properties which are used in the forthcoming proofs, namely

$$\mathscr{P}^1(K) \subset V_h\big|_K , \quad \mathscr{P}^1(K) \subset V_h^{\text{ref}}\big|_K \qquad \text{and} \qquad 0 \le \psi_{\mathbf{z}}, \psi_{\mathbf{z}}^{\text{ref}} \le 1, \tag{3.12}$$

where $\psi_{\mathbf{z}}$ and $\psi_{\mathbf{z}}^{\text{ref}}$ denote the corresponding nodal basis functions of V_h and V_h^{ref}, respectively.

3.4.3 Anisotropic Trace Inequality and Best Approximation

In this section we transfer some of the results of Sect. 3.2 to the regime of anisotropic meshes. Here, the mapping (3.8) is employed to transform a regular and stable anisotropic element K onto its reference configuration $\widehat{K}$, which is regular and stable in the sense of Sect. 2.2, see also Remark 3.12.

Lemma 3.21 (Anisotropic Trace Inequality) *Let $K \in \mathscr{K}_h$ be a polytopal element of a regular and stable anisotropic mesh $\mathscr{K}_h$ with edge ($d = 2$) or face ($d = 3$) $F \in \mathscr{F}_h$, $F \subset \partial K$. It holds*

$$\|v\|^2_{L_2(F)} \le c\, \frac{|F|}{|K|} \left(\|v\|^2_{L_2(K)} + \|A_K^{-\top}\nabla v\|^2_{L_2(K)} \right) ,$$

where the constant c only depends on the regularity and stability parameters of the mesh.

Proof In order to prove the estimate, we make use of the transformation (3.8) to the reference configuration $\widehat{K}$ with $\widehat{v} = v \circ \mathfrak{F}_K^{-1}$, a trace inequality on $\widehat{K}$, see Lemma 3.3,

as well as of (3.10), (3.11) and $h_{\widehat{K}}^{-d} \leq |\widehat{K}|^{-1} = 1$. These tools yield

$$\begin{aligned}
\|v\|_{L_2(F)}^2 &= \frac{|F|}{|\widehat{F}|}\|\widehat{v}\|_{L_2(\widehat{F})}^2 \\
&\leq c\frac{|F|}{|\widehat{F}|}\left(h_{\widehat{K}}^{-1}\|\widehat{v}\|_{L_2(\widehat{K})}^2 + h_{\widehat{K}}|\widehat{v}|_{H^1(\widehat{K})}^2\right) \\
&\leq c|F|h_{\widehat{K}}^{-d}\left(\|\widehat{v}\|_{L_2(\widehat{K})}^2 + h_{\widehat{K}}^2|\widehat{v}|_{H^1(\widehat{K})}^2\right) \\
&\leq c|F|\left(\|\widehat{v}\|_{L_2(\widehat{K})}^2 + \|\widehat{\nabla}\widehat{v}\|_{L_2(\widehat{K})}^2\right) \\
&= c\frac{|F|}{|K|}\left(\|v\|_{L_2(K)}^2 + \|A_K^{-\top}\nabla v\|_{L_2(K)}^2\right) .
\end{aligned}$$

□

Remark 3.22 If we plug in the definition of $A = \alpha_K \Lambda_K^{-1/2} U_K^\top$, we have the anisotropic trace inequality

$$\|v\|_{L_2(F)}^2 \leq c\frac{|F|}{|K|}\left(\|v\|_{L_2(K)}^2 + \|\alpha_K^{-1}\Lambda_K^{1/2}U_K^\top\nabla v\|_{L_2(K)}^2\right) .$$

Obviously, the derivatives of v in the characteristic directions $\mathbf{u}_{K,j}$ are scaled by the characteristic lengths $\lambda_j^{1/2}$, $j = 1, \ldots, d$ of the element K. This seems to be appropriate for functions with anisotropic behaviour which are aligned with the mesh.

For later comparisons with other methods, we bound the term $|F|/|K|$ in case of $F \subset \partial K$. Let $\mathbf{z}_{\widehat{K}}$ be the midpoint of the circle/ball in Definitions 2.1 and 2.11, respectively, of the regular and stable reference configuration $\widehat{K}$. Obviously, it is $|K| \geq |P|$ for the d-dimensional pyramid P with base side F and apex point $\mathfrak{F}_K^{-1}(z_{\widehat{K}})$, since $P \subset K$ due to the linearity of $\mathfrak{F}_K$. Denote by $h_{P,F}$ the hight of this pyramid, then it is $|P| = \frac{1}{3}|F|h_{P,F}$ and we obtain

$$\frac{|F|}{|K|} \leq ch_{P,F}^{-1} . \tag{3.13}$$

In the derivation of approximation estimates, the Poincaré constant also plays a crucial role on anisotropic meshes. This constant is given in (3.4).

Lemma 3.23 *Let $\mathscr{K}_h$ be a regular and stable anisotropic mesh, $\omega_{\mathbf{z}}$ and ω_K be neighbourhoods as described in Sect. 3.1, and $K \in \mathscr{K}_h$ with $K \subset \omega_{\mathbf{z}}$. The Poincaré constants $C_P(\widetilde{\omega}_{\mathbf{z}})$ and $C_P(\widetilde{\omega}_K)$ for the mapped patches $\widetilde{\omega}_{\mathbf{z}} = \mathfrak{F}_K(\omega_{\mathbf{z}})$ as well as $\widetilde{\omega}_K = \mathfrak{F}_K(\omega_K)$, can be bounded uniformly depending only on the regularity and stability parameters of the mesh.*

Proof According to Lemma 3.15 and Proposition 3.17, the patches $\widetilde{\omega}_{\mathbf{z}}$ and $\widetilde{\omega}_K$ consist of regular and stable polytopal elements. Thus, we utilize Lemma 3.5 on the mapped patches and the statement follows. □

Next, we derive a best approximation result on patches of anisotropic elements.

Lemma 3.24 *Let $\mathscr{K}_h$ be a regular and stable anisotropic mesh with node $\mathbf{z} \in \mathscr{N}_h$ and element $K \in \mathscr{K}_h$. Furthermore, let $\omega_{\mathbf{z}}$ and ω_K be the neighbourhood of $\mathbf{z}$ and K, respectively, and we assume $K \subset \omega_{\mathbf{z}}$. For $\omega \in \{\omega_{\mathbf{z}}, \omega_K\}$ it holds*

$$\|v - \Pi_\omega v\|_{L_2(\omega)} \leq c \, \|A_K^{-\top} \nabla v\|_{L_2(\omega)} \, ,$$

and furthermore

$$\|v - \Pi_\omega v\|_{L_2(\omega)} \leq c \left(\sum_{K' \in \mathscr{K}_h : K' \subset \omega} \|A_{K'}^{-\top} \nabla v\|^2_{L_2(K')} \right)^{1/2} ,$$

where the constant c only depends on the regularity and stability parameters of the mesh.

Proof We make use of the mapping (3.8) and indicate the objects on the mapped geometry with a tilde, e.g., $\widetilde{\omega} = \mathfrak{F}_K(\omega)$. Furthermore, we exploited that the mapped L_2-projection coincides with the L_2-projection on the mapped patch, consequently $\widetilde{\Pi_\omega v} = \Pi_{\widetilde{\omega}} \widetilde{v}$. This yields together with Lemma 3.23

$$\begin{aligned} \|v - \Pi_\omega v\|_{L_2(\omega)} &= |K|^{1/2} \, \|\widetilde{v} - \Pi_{\widetilde{\omega}} \widetilde{v}\|_{L_2(\widetilde{\omega})} \\ &\leq c h_{\widetilde{\omega}} |K|^{1/2} \, |\widetilde{v}|_{H^1(\widetilde{\omega})} \\ &= c h_{\widetilde{\omega}} |K|^{1/2} \, \|\widetilde{\nabla} \widetilde{v}\|_{L_2(\widetilde{\omega})} \\ &= c h_{\widetilde{\omega}} \, \|A_K^{-\top} \nabla v\|_{L_2(\omega)} \, . \end{aligned}$$

The term $h_{\widetilde{\omega}}$ is uniformly bounded according to Lemma 3.20, and thus the first estimate is proven.

In order to prove the second estimate, we employ the first one and write

$$\|v - \Pi_\omega v\|^2_{L_2(\omega)} \leq c \, \|A_K^{-\top} \nabla v\|^2_{L_2(\omega)} = c \sum_{K' \in \mathscr{K}_h : K' \subset \omega} \|A_K^{-\top} \nabla v\|^2_{L_2(K')} \, .$$

Therefore, it remains to estimate $\|A_K^{-\top} \nabla v\|_{L_2(K')}$ by $\|A_{K'}^{-\top} \nabla v\|_{L_2(K')}$ for any element $K' \subset \omega$. We make use of the mesh regularity and stability, see Definition 3.13,

and proceed similar as in the proof of Lemma 3.15.

$$\begin{aligned}
\|A_K^{-\top}\nabla v\|_{L_2(K')} &= \frac{\alpha_{K'}}{\alpha_K}\|\alpha_{K'}^{-1}((I+\Delta^{K',K})\Lambda_{K'})^{1/2}(R^{K',K}U_{K'})^\top\nabla v\|_{L_2(K')} \\
&= \frac{\alpha_{K'}}{\alpha_K}\|\alpha_{K'}^{-1}(I+\Delta^{K',K})^{1/2}\Lambda_{K'}^{1/2}U_{K'}^\top(R^{K',K})^\top\nabla v\|_{L_2(K')} \\
&= \frac{\alpha_{K'}}{\alpha_K}\|\alpha_{K'}^{-1}(I+\Delta^{K',K})^{1/2}\Lambda_{K'}^{1/2}U_{K'}^\top(R^{K',K})^\top U_{K'}\Lambda_{K'}^{-1/2}\Lambda_{K'}^{1/2}U_{K'}^\top\nabla v\|_{L_2(K')} \\
&\le \frac{\alpha_{K'}}{\alpha_K}\|(I+\Delta^{K',K})^{1/2}\Lambda_{K'}^{1/2}U_{K'}^\top(R^{K',K})^\top U_{K'}\Lambda_{K'}^{-1/2}\|_2\|A_{K'}^{-\top}\nabla v\|_{L_2(K')}\,,
\end{aligned}$$

where we substituted $A_K^{-\top} = \alpha_{K'}^{-1}\Lambda_{K'}^{1/2}U_{K'}^\top$. Finally, we have to bound the ratio $\alpha_{K'}/\alpha_K$ and the matrix norm. According to the choice (3.9) and Lemma 3.20, it is

$$\begin{aligned}
\left(\frac{\alpha_{K'}}{\alpha_K}\right)^2 &= \frac{|K|\sqrt{\prod_{j=1}^d \lambda_{K',j}}}{|K'|\sqrt{\prod_{j=1}^d \lambda_{K,j}}} = \frac{|K|\sqrt{\prod_{j=1}^d (1+\delta_j^{K,K'})\lambda_{K,j}}}{|K'|\sqrt{\prod_{j=1}^d \lambda_{K,j}}} \\
&\le (1+c_\delta)^{d/2}\frac{|K|}{|K'|} \le c\,,
\end{aligned}$$

and for the matrix norm, we have

$$\begin{aligned}
&\|(I+\Delta^{K',K})^{1/2}\Lambda_{K'}^{1/2}U_{K'}^\top(R^{K',K})^\top U_{K'}\Lambda_{K'}^{-1/2}\|_2 \\
&\le \|(I+\Delta^{K',K})^{1/2}\|_2\|\Lambda_{K'}^{1/2}U_{K'}^\top(R^{K',K}-I)^\top U_{K'}\Lambda_{K'}^{-1/2}+I\|_2 \\
&\le \sqrt{1+c_\delta}(1+c_R)\,,
\end{aligned}$$

that finishes the proof. □

Remark 3.25 In the previous proof, we have seen in particular that for neighbouring elements $K, K' \subset \omega_K$, it is

$$\|A_K^{-\top}\nabla v\|_{L_2(K')} \le c\,\|A_{K'}^{-\top}\nabla v\|_{L_2(K')}$$

with a constant depending only on the regularity and stability of the mesh.

3.4.4 *Quasi-Interpolation of Anisotropic Non-smooth Functions*

In this section, we consider the quasi-interpolation operators from Sect. 3.3 on anisotropic polygonal and polyhedral meshes. The analysis relies on the mapping to the reference configuration of regular and stable anisotropic polytopal elements as

in [181]. Earlier results for quasi-interpolation operators on anisotropic simplicial meshes can be found in [10, 79, 119], for example. Some comparisons are also drawn in the following.

The general form of the Clément and to Scott–Zhang operator is given in (3.6) for $v \in H^1(\Omega)$, namely

$$\mathfrak{I} v = \sum_{\mathbf{z} \in \mathscr{N}_*} (\Pi_{\omega(\psi_\mathbf{z})} v) \psi_\mathbf{z} \in V_h \ ,$$

where the set of nodes $\mathscr{N}_*$ and the neighbourhoods $\omega(\psi_\mathbf{z})$ are chosen accordingly. We point out, that the results of this section stay valid if we replace the basis functions $\psi_\mathbf{z}$ by $\psi_\mathbf{z}^{\mathrm{ref}}$, which have been discussed in Sect. 3.4.2. In this case the quasi-interpolation operator maps into the approximation space defined with the help of the reference configurations, i.e. $\mathfrak{I} : H^1(\Omega) \to V_h^{\mathrm{ref}}$. In the forthcoming proofs, we only employ the properties (3.12) which are shared by V_h and V_h^{ref}.

3.4.4.1 Clément-Type Interpolation

The Clément interpolation operator $\mathfrak{I}_C$ is defined by (3.6) with $\mathscr{N}_* = \mathscr{N}_h \setminus \mathscr{N}_{h,D}$ and $\omega(\psi_\mathbf{z}) = \omega_\mathbf{z}$, see Sect. 3.3.1 for details. For $v \in H^1_D(\Omega)$, it is $\mathfrak{I}_C v \in H^1_D(\Omega)$ by construction.

Theorem 3.26 *Let $\mathscr{K}_h$ be a regular and stable anisotropic mesh and $K \in \mathscr{K}_h$. The Clément interpolation operator satisfies for $v \in H^1_D(\Omega)$ the interpolation error estimate*

$$\|v - \mathfrak{I}_C v\|_{L_2(K)} \leq c \, \|A_K^{-\top} \nabla v\|_{L_2(\omega_K)} \ ,$$

and for an edge/face $F \in \mathscr{F}(K) \setminus \mathscr{F}_{h,D}$

$$\|v - \mathfrak{I}_C v\|_{L_2(F)} \leq c \, \frac{|F|^{1/2}}{|K|^{1/2}} \, \|A_K^{-\top} \nabla v\|_{L_2(\omega_F)} \ ,$$

where the constants c only depend on the regularity and stability parameters of the mesh.

Proof We can follow classical arguments as for isotropic meshes, cf. Theorem 3.7. The main ingredients are the observation that the basis functions $\psi_\mathbf{z}$ form a partition of unity on $\overline{K}$, and that they are bounded by one. Furthermore, anisotropic approximation estimates, see Lemma 3.24, the anisotropic trace inequality in Lemmata 3.21 and 3.20 and Remark 3.25 are employed. We only sketch the proof of the second estimate.

The partition of unity property is used, which also holds on each edge/face F, i.e. $\sum_{\mathbf{z} \in \mathscr{N}(F)} \psi_\mathbf{z} = 1$ on $\overline{F}$. We distinguish two cases, first let $\mathscr{N}(F) \cap \mathscr{N}_{h,D} = \varnothing$.

With the help of Lemmata 3.21 and 3.24, we obtain

$$\begin{aligned}\|v - \mathfrak{I}_C v\|_{L_2(F)} &= \sum_{\mathbf{z}\in\mathscr{N}(F)} \|\psi_{\mathbf{z}}(v - \Pi_{\omega_{\mathbf{z}}} v)\|_{L_2(F)} \;\le \sum_{\mathbf{z}\in\mathscr{N}(F)} \|v - \Pi_{\omega_{\mathbf{z}}} v\|_{L_2(F)} \\ &\le c \sum_{\mathbf{z}\in\mathscr{N}(F)} \frac{|F|^{1/2}}{|K|^{1/2}} \left(\|v - \Pi_{\omega_{\mathbf{z}}} v\|^2_{L_2(K)} + \|A_K^{-\top} \nabla v\|^2_{L_2(K)} \right)^{1/2} \\ &\le c \sum_{\mathbf{z}\in\mathscr{N}(F)} \frac{|F|^{1/2}}{|K|^{1/2}} \, \|A_K^{-\top} \nabla v\|_{L_2(\omega_{\mathbf{z}})} .\end{aligned}$$

For the second case with $\mathscr{N}(F) \cap \mathscr{N}_{h,D} \neq \varnothing$, we find

$$\|v - \mathfrak{I}_C v\|_{L_2(F)} \le \sum_{\mathbf{z}\in\mathscr{N}(F)} \|\psi_{\mathbf{z}}(v - \Pi_{\omega_{\mathbf{z}}} v)\|_{L_2(F)} + \sum_{\mathbf{z}\in\mathscr{N}(F)\cap\mathscr{N}_{h,D}} \|\psi_{\mathbf{z}} \Pi_{\omega_{\mathbf{z}}} v\|_{L_2(F)} . \tag{3.14}$$

The first sum has already been estimated, thus we consider the term in the second sum. For $\mathbf{z} \in \mathscr{N}(F) \cap \mathscr{N}_{h,D}$, i.e. $\mathbf{z} \in \overline{\Gamma}_D$, there is an element $K' \subset \omega_{\mathbf{z}}$ and an edge/face $F' \in \mathscr{F}(K')$ such that $\mathbf{z} \in \mathscr{N}(F')$ and $F' \in \mathscr{F}_{h,D}$. Since v vanishes on F', Lemmata 3.21 and 3.24 as well as Remark 3.25 yield

$$|\Pi_{\omega_{\mathbf{z}}} v| = |F'|^{-1/2} \, \|v - \Pi_{\omega_{\mathbf{z}}} v\|_{L_2(F')} \le c \, |K'|^{-1/2} \, \|A_K^{-\top} \nabla v\|_{L_2(\omega_{\mathbf{z}})} .$$

Because $|K'|/|K|$ is uniformly bounded according to Lemma 3.20, we obtain

$$\|\psi_{\mathbf{z}} \Pi_{\omega_{\mathbf{z}}} v\|_{L_2(F)} \le |\Pi_{\omega_{\mathbf{z}}} v| \, \|\psi_{\mathbf{z}}\|_{L_\infty(F)} \, |F|^{1/2} \le c \, \frac{|F|^{1/2}}{|K|^{1/2}} \, \|A_K^{-\top} \nabla v\|_{L_2(\omega_{\mathbf{z}})} .$$

Finally, since the number of nodes per element is uniformly bounded according to Proposition 3.18, this estimate as well as the one derived in the first case applied to (3.14) yield the second interpolation error estimate in the theorem. □

Remark 3.27 In the case of an isotropic polytopal element K with edge/face F it is

$$\lambda_1 \approx \ldots \approx \lambda_d \sim h_K^2 , \quad \text{and thus} \quad \alpha_K \sim 1 .$$

Therefore, we obtain from Theorem 3.26 with $A_K^{-\top} = \alpha_K^{-1} \Lambda_K^{1/2} U_K^\top$ that

$$\|v - \mathfrak{I}_C v\|_{L_2(K)} \le c h_K \, \|U_K^\top \nabla v\|_{L_2(\omega_K)} = c h_K \, |v|_{H^1(\omega_K)} ,$$

and

$$\|v - \mathfrak{I}_C v\|_{L_2(F)} \le c \, \frac{h_K |F|^{1/2}}{|K|^{1/2}} \, \|U_K^\top \nabla v\|_{L_2(\omega_F)} \le c h_F^{1/2} \, |v|_{H^1(\omega_F)} ,$$

since $|F| \leq h_F^{d-1}$ as well as $|K| \geq c h_K^d$ and $h_K \leq c h_F$ in consequence of the regularity and stability, cf. Remark 3.12. Obviously, we recover the classical interpolation error estimates for the Clément interpolation operator, cf. Theorem 3.7.

In the following, we rewrite our results in order to compare them with the work of Formaggia and Perotto [79]. It is $A_K^{-\top} = \alpha_K^{-1} \Lambda_K^{1/2} U_K^\top$ with $U_K = (\mathbf{u}_{K,1}, \ldots, \mathbf{u}_{K,d})$. Thus, we observe

$$\|A_K^{-\top} \nabla v\|_{L_2(\omega_K)}^2 = \alpha_K^{-2} \sum_{j=1}^d \lambda_{K,j} \, \|\mathbf{u}_{K,j} \cdot \nabla v\|_{L_2(\omega_K)}^2 \,,$$

and since $\mathbf{u}_{K,j} \cdot \nabla v : \mathbb{R}^d \to \mathbb{R}$, we obtain

$$\|\mathbf{u}_{K,j} \cdot \nabla v\|_{L_2(\omega_K)}^2 = \sum_{K' \subset \omega_K} \int_{K'} \mathbf{u}_{K,j}^\top \nabla v (\nabla v)^\top \mathbf{u}_{K,j} \, \mathrm{d}\mathbf{x} = \mathbf{u}_{K,j}^\top \, G_K(v) \, \mathbf{u}_{K,j}$$

with

$$G_K(v) = \sum_{K' \subset \omega_K} \left(\int_{K'} \frac{\partial v}{\partial x_i} \frac{\partial v}{\partial x_j} \, \mathrm{d}\mathbf{x} \right)_{i,j=1}^d \in \mathbb{R}^{d \times d} \,, \quad \mathbf{x} = (x_1, \ldots, x_d)^\top \,.$$

Therefore, we can deduce from Theorem 3.26 an equivalent formulation.

Proposition 3.28 *Let $\mathscr{K}_h$ be a regular and stable anisotropic mesh and $K \in \mathscr{K}_h$. The Clément interpolation operator satisfies for $v \in H_D^1(\Omega)$ the interpolation error estimate*

$$\|v - \mathfrak{I}_C v\|_{L_2(K)} \leq c \, \alpha_K^{-1} \left(\sum_{j=1}^d \lambda_{K,j} \, \mathbf{u}_{K,j}^\top \, G_K(v) \, \mathbf{u}_{K,j} \right)^{1/2} \,,$$

and for an edge/face $F \in \mathscr{F}(K) \setminus \mathscr{F}_{h,D}$

$$\|v - \mathfrak{I}_C v\|_{L_2(F)} \leq c \, \alpha_K^{-1} \, \frac{|F|^{1/2}}{|K|^{1/2}} \left(\sum_{j=1}^d \lambda_{K,j} \, \mathbf{u}_{K,j}^\top \, G_K(v) \, \mathbf{u}_{K,j} \right)^{1/2} \,,$$

where the constant c only depends on the regularity and stability parameters of the mesh.

Now we are ready to compare the interpolation error estimates with the ones derived by Formaggia and Perotto. These authors considered the case of anisotropic triangular meshes in two-dimensions, i.e. $d = 2$. The inequalities in Proposition 3.28 correspond to the derived estimates (2.12) and (2.15) in [79] but they are

valid on much more general meshes. When comparing these estimates to the results of Formaggia and Perotto, one has to take care on the powers of the lambdas. The triangular elements in their works are scaled with $\lambda_{i,K}$, $i = 1, 2$ in the characteristic directions whereas the scaling in this section is $\lambda_{K,i}^{1/2}$, $i = 1, 2$.

Obviously, the first inequality of the previous proposition corresponds to the derived estimate (2.12) in [79] up to the scaling factor α_K^{-1}. However, for convex elements the assumption

$$\alpha_K \sim 1 \,, \qquad \text{i.e.,} \qquad |K| \sim \sqrt{\lambda_{K,1}\lambda_{K,2}} \,,$$

seems to be convenient, since this means that the area $|K|$ of the element is proportional to the area $\pi\sqrt{\lambda_{K,1}}\sqrt{\lambda_{K,2}}$ of the inscribed ellipse, which is given by the scaled characteristic directions of the element.

In order to recognize the relation of the second inequality under these assumptions, we estimate the term $|F|/|K|$ by (3.13) and by applying $h_{P,F} \geq \lambda_{K,2}^{1/2}$. This yields

$$\|v - \mathfrak{I}_C v\|_{L_2(F)} \leq c \left(\frac{1}{\lambda_{K,2}^{1/2}}\right)^{1/2} \left(\lambda_{K,1}\, \mathbf{u}_{K,1}^\top G_K(v)\, \mathbf{u}_{K,1} + \lambda_{K,2}\, \mathbf{u}_{K,2}^\top G_K(v)\, \mathbf{u}_{K,2}\right)^{1/2},$$

and shows the correspondence to [79], since h_K and $\lambda_{1,K}$ are proportional in the referred work.

3.4.4.2 Scott–Zhang-Type Interpolation

The Scott–Zhang interpolation operator $\mathfrak{I}_{SZ} : H^1(\Omega) \to V_h$ is defined by (3.6) with $\mathcal{N}_* = \mathcal{N}$ and $\omega(\psi_{\mathbf{z}}) = F_{\mathbf{z}}$, where $F_{\mathbf{z}} \in \mathcal{F}_h$ is an edge ($d = 2$) or face ($d = 3$) with $\mathbf{z} \in \overline{F}_{\mathbf{z}}$ and

$$F_{\mathbf{z}} \subset \Gamma_D \text{ if } \mathbf{z} \in \overline{\Gamma}_D \qquad \text{and} \qquad F_{\mathbf{z}} \subset \Omega \cup \Gamma_N \text{ if } \mathbf{z} \in \Omega \cup \Gamma_N \,.$$

By construction, it is $\mathfrak{I}_{SZ} v \in H_D^1(\Omega)$ for $v \in H_D^1(\Omega)$, such that homogeneous Dirichlet data is preserved. We have the following local stability result on anisotropic meshes.

Lemma 3.29 *Let $\mathcal{K}_h$ be a regular and stable anisotropic mesh and $K \in \mathcal{K}_h$. The Scott–Zhang interpolation operator satisfies for $v \in H^1(\Omega)$ the local stability*

$$\|\mathfrak{I}_{SZ} v\|_{L_2(K)} \leq c \left(\|v\|_{L_2(\omega_K)} + \|A_K^{-\top} \nabla v\|_{L_2(\omega_K)}\right) \,,$$

where the constant c only depends on the regularity and stability parameters of the mesh.

Proof The proof is analog to the isotropic version in Lemma 3.8. The difference is that the anisotropic trace inequality Lemmata 3.21 and 3.20, Remark 3.25 and Proposition 3.18 are used. For details see [181]. □

Theorem 3.30 *Let $\mathscr{K}_h$ be a regular and stable anisotropic mesh and $K \in \mathscr{K}_h$. The Scott–Zhang interpolation operator satisfies for $v \in H^1(\Omega)$ the interpolation error estimate*

$$\|v - \mathfrak{I}_{SZ} v\|_{L_2(K)} \leq \|A_K^{-\top} \nabla v\|_{L_2(\omega_K)} ,$$

where the constant c only depends on the regularity and stability parameters of the mesh.

Proof For $p = \Pi_{\omega_K} v \in \mathbb{R}$ it is obviously $p = \mathfrak{I}_{SZ} p$ and $\nabla p = 0$. The estimate in the theorem follows by Lemma 3.29 and the application of Lemma 3.24, since

$$\begin{aligned} \|v - \mathfrak{I}_{SZ} v\|_{L_2(K)} &\leq \|v - p\|_{L_2(K)} + \|\mathfrak{I}_{SZ}(v - p)\|_{L_2(K)} \\ &\leq c \left(\|v - p\|_{L_2(\omega_K)} + \|A_K^{-\top} \nabla v\|_{L_2(\omega_K)} \right) \\ &\leq c \, \|A_K^{-\top} \nabla v\|_{L_2(\omega_K)} . \end{aligned}$$

□

3.4.5 *Interpolation of Anisotropic Smooth Functions*

In the previous section, we considered quasi-interpolation of functions in $H^1(\Omega)$. However, we may also address classical interpolation employing point evaluations in the case that the function to be interpolated is sufficiently regular as in Sect. 2.4. This is possible for functions in $H^2(\Omega)$. In the following, we consider the pointwise interpolation of lowest order with $k = 1$ into the approximation space V_h^{ref} on anisotropic meshes. V_h^{ref} has been discussed in Sect. 3.4.2 and its basis functions $\psi_{\mathbf{z}}^{\text{ref}}$ are constructed such that $\widehat{\psi}_{\mathbf{z}}^{\text{ref}}$ coincide on the reference configuration $\widehat{K}$ with the usual harmonic basis functions from Sect. 2.3. The interpolation operator is given as

$$\mathfrak{I}_h v = \sum_{\mathbf{z} \in \mathscr{N}_h} v(\mathbf{z}) \, \psi_{\mathbf{z}}^{\text{ref}} \in V_h^{\text{ref}} \tag{3.15}$$

for $v \in H^2(\Omega)$, on anisotropic meshes. In the analysis, it is sufficient to study the restriction of $\mathfrak{I}_h : H^2(\Omega) \to V_h^{\text{ref}}$ onto a single element $K \in \mathscr{K}_h$ and we denote this restriction by the same symbol

$$\mathfrak{I}_h : H^2(K) \to V_h^{\text{ref}}|_K .$$

Furthermore, we make use of the mapping to and from the reference configuration, cf. (3.8). As earlier, we mark the operators and functions defined over the reference configuration by a hat, as, for instance, $\widehat{v} = v \circ \mathfrak{F}_K^{-1} : \widehat{K} \to K$. We have already used $\nabla v = \alpha_K U_K \Lambda_K^{-1/2} \widehat{\nabla} \widehat{v}$, and by employing some calculus we find

$$\widehat{H}(\widehat{v}) = \alpha_K^{-2} \Lambda_K^{1/2} U_K^\top H(v) U_K \Lambda_K^{1/2} , \tag{3.16}$$

where $H(v)$ denotes the Hessian matrix of $v \in H^2(\Omega)$ and $\widehat{H}(\widehat{v})$ the corresponding Hessian on the reference configuration. Additionally, we observe the relation between the interpolation $\mathfrak{I}_h v$ transferred to the reference configuration $\widehat{K}$ and the interpolation $\widehat{\mathfrak{I}}_h \widehat{v}$ defined directly on $\widehat{K}$. Namely, it is

$$\widehat{\mathfrak{I}_h v} = \widehat{\mathfrak{I}}_h \widehat{v} , \tag{3.17}$$

since only function evaluations in the nodes are involved and the mapped basis functions coincide with the basis functions defined directly on $\widehat{K}$, see Sect. 3.4.2. Furthermore, the interpolation $\widehat{\mathfrak{I}}_h$ coincides with the pointwise interpolation in Sect. 2.4 since the functions $\widehat{\psi}_{\mathbf{z}}^{\mathrm{ref}}$ are harmonic. Thus, we can apply known results for the interpolation error on the reference configuration.

First, we consider the scaling of the H^1-seminorm when K is mapped to $\widehat{K}$.

Lemma 3.31 *Let $K \in \mathscr{K}_h$ be a polytopal element of a regular and stable anisotropic mesh $\mathscr{K}_h$. For $v \in H^1(K)$, it is*

$$\sqrt{\frac{\prod_{j=2}^d \lambda_{K,j}}{\lambda_{K,1}}}\, |\widehat{v}|^2_{H^1(\widehat{K})} \le |v|^2_{H^1(K)} \le \sqrt{\frac{\prod_{j=1}^{d-1} \lambda_{K,j}}{\lambda_{K,d}}}\, |\widehat{v}|^2_{H^1(\widehat{K})} .$$

Proof Applying the transformation to the reference configuration yields

$$\begin{aligned} |v|^2_{H^1(K)} &= \|\nabla v\|^2_{L_2(K)} = |K|\, \|\alpha_K U_K \Lambda_K^{-1/2} \widehat{\nabla} \widehat{v}\|^2_{L_2(\widehat{K})} \\ &= |K| \alpha_K^2\, \|\Lambda_K^{-1/2} \widehat{\nabla} \widehat{v}\|^2_{L_2(\widehat{K})} = |K| \alpha_K^2 \sum_{j=1}^d \lambda_{K,j}^{-1} \left\| \frac{\partial \widehat{v}}{\partial \widehat{x}_j} \right\|^2_{L_2(\widehat{K})} . \end{aligned}$$

Since $\lambda_{K,1} \ge \ldots \ge \lambda_{K,d}$, we obtain

$$\frac{|K| \alpha_K^2}{\lambda_{K,1}}\, |\widehat{v}|^2_{H^1(\widehat{K})} \le |v|^2_{H^1(K)} \le \frac{|K| \alpha_K^2}{\lambda_{K,d}}\, |\widehat{v}|^2_{H^1(\widehat{K})} .$$

Due to the choice (3.9) for α_K, it is $|K| \alpha_K^2 = \sqrt{\prod_{j=1}^d \lambda_{K,j}}$, that completes the proof. □

Next, we address the interpolation error. Therefore, we use the convention that $H^0(K) = L_2(K)$.

Theorem 3.32 *Let $K \in \mathscr{K}_h$ be a polytopal element of a regular and stable anisotropic mesh $\mathscr{K}_h$. For $v \in H^2(\Omega)$, it is*

$$|v - \mathfrak{I}_h v|^2_{H^\ell(K)} \leq c\alpha_K^{-4}\, S_\ell(K) \sum_{i,j=1}^{d} \lambda_{K,i}\lambda_{K,j} L_K(\mathbf{u}_{K,i}, \mathbf{u}_{K,j}; v)$$

with

$$S_\ell(K) = \begin{cases} 1, & \text{for } \ell = 0, \\ \dfrac{1}{|K|}\sqrt{\dfrac{\prod_{j=1}^{d-1}\lambda_{K,j}}{\lambda_{K,d}}}, & \text{for } \ell = 1, \end{cases}$$

where

$$L_K(\mathbf{u}_{K,i}, \mathbf{u}_{K,j}; v) = \int_K \left(\mathbf{u}_{K,i}^\top H(v)\mathbf{u}_{K,j}\right)^2 \mathrm{d}\mathbf{x} \quad \text{for } i, j = 1, \ldots, d\ .$$

and the constant c only depends on the regularity and stability parameters of the mesh.

Proof Property (3.17) together with the scaling to the reference configuration and Lemma 3.31 as well as (3.10) yield for $\ell = 0, 1$

$$\begin{aligned} |v - \mathfrak{I}_h v|^2_{H^\ell(K)} &\leq |K|\ S_\ell(K)\ |\widehat{v} - \widehat{\mathfrak{I}}_h\widehat{v}|^2_{H^\ell(\widehat{K})} \\ &\leq c h_{\widehat{K}}^{2(2-\ell)} |K|\ S_\ell(K)\ |\widehat{v}|^2_{H^2(\widehat{K})} \\ &\leq c|K|\ S_\ell(K)\ |\widehat{v}|^2_{H^2(\widehat{K})}\ , \end{aligned}$$

where the interpolation estimate in Theorem 2.27 has been applied on $\widehat{K}$. Next, we transform the H^2-semi-norm back to the element K. Employing the mapping and the relation (3.16) gives

$$\begin{aligned} |\widehat{v}|^2_{H^2(\widehat{K})} &= \int_{\widehat{K}} \|\widehat{H}(\widehat{v})\|_F^2 \,\mathrm{d}\widehat{\mathbf{x}} \\ &= \frac{\alpha_K^{-4}}{|K|} \int_K \|\Lambda_K^{1/2} U_K^\top H(v) U_K \Lambda_K^{1/2}\|_F^2 \,\mathrm{d}\mathbf{x}\ , \end{aligned}$$

where $\|\cdot\|_F$ denotes the Frobenius norm of a matrix. A small exercise yields

$$\|\Lambda_K^{1/2} U_K^\top H(v) U_K \Lambda_K^{1/2}\|_F^2 = \sum_{i,j=1}^{d} \lambda_{K,i}\lambda_{K,j} \left(\mathbf{u}_{K,i}^\top H(v)\mathbf{u}_{K,j}\right)^2 ,$$

and consequently

$$|\widehat{v}|_{H^2(\widehat{K})}^2 = \frac{\alpha_K^{-4}}{|K|} \sum_{i,j=1}^{d} \lambda_{K,i}\lambda_{K,j} L_K(\mathbf{u}_{K,i}, \mathbf{u}_{K,j}; v) .$$

Combining the derived results yields the desired estimates. □

For the comparison with the work of Formaggia and Perotto developed in two-dimensions, we remember that their lambdas behave like $\lambda_{i,K} \sim \sqrt{\lambda_{K,i}}$, $i = 1, 2$. Employing the assumption $\alpha_K \sim 1$ raised in the comparison of Sect. 3.3.1, we find

$$\frac{\sqrt{\lambda_{K,1}/\lambda_{K,2}}}{|K|} \sim \frac{1}{\lambda_{K,2}} .$$

Therefore, we recognize that the estimates in Theorem 3.32 match the results of Lemma 2 in [79], but on much more general meshes.

3.4.6 *Numerical Assessment of Anisotropic Meshes*

In the introduction of Sect. 3.4, we already mentioned that polygonal and polyhedral meshes are much more flexible in meshing than classical finite element shapes. This is in particular true for the generation of anisotropic meshes. In this section we give a first numerical assessment on polytopal anisotropic mesh refinement. We propose a bisection approach that does not rely on any initially prescribed direction and which is applicable in two- and three-dimensions. Classical bisection approaches for triangular and tetrahedral meshes do not share this versatility and they have to be combined with additional strategies like edge swapping, node removal and local node movement, see [152].

Starting from the local interpolation error estimate in Theorem 3.26, we obtain the global version

$$\|v - \mathfrak{I}_C v\|_{L_2(\Omega)} \leq c \left(\sum_{K \in \mathscr{K}_h} \|A_K^{-\top} \nabla v\|_{L_2(K)}^2 \right)^{1/2}$$

by exploiting Remark 3.25 and Proposition 3.18. As in the derivation of Proposition 3.28, we easily see that

$$\eta = \sqrt{\sum_{K \in \mathscr{K}_h} \eta_K^2} \qquad \text{with} \qquad \eta_K^2 = \alpha_K^{-2} \sum_{j=1}^{d} \lambda_{K,j}\, \mathbf{u}_{K,j}^\top\, G_K^*(v)\, \mathbf{u}_{K,j}$$

and

$$G_K^*(v) = \left(\int_K \frac{\partial v}{\partial x_i} \frac{\partial v}{\partial x_j}\, \mathrm{d}\mathbf{x} \right)_{i,j=1}^{d} \in \mathbb{R}^{d \times d}\,, \quad \mathbf{x} = (x_1, \ldots, x_d)^\top$$

is a good error measure and the local values η_K may serve as error indicators over the polytopal elements. This estimate also remains meaningful on isotropic polytopal meshes, cf. Remark 3.27. In the case that $v \in H^1(\Omega)$ and its derivatives are known, we can thus apply the following adaptive mesh refinement algorithm:

1. Let $\mathscr{K}_0$ be a given initial mesh and $\ell = 0$.
2. Compute the error indicators η_K and η with the knowledge of the exact function v and its derivatives.
3. Mark all elements K for refinement which satisfy $\eta_K > 0.95\eta/\sqrt{|\mathscr{K}_\ell|}$, where $|\mathscr{K}_\ell|$ is the number of elements in the current mesh.
4. Refine the marked elements as described below in order to obtain a refined mesh $\mathscr{K}_{\ell+1}$.
5. Go to 2.

In step 3, we have chosen a equidistribution strategy which marks all elements for refinement whose error indicator is larger than the mean value. The factor 0.95 has been chosen for stabilizing reasons in the computations when the error is almost uniformly distributed. For the refinement in step 4, we have a closer look at the first term in the sum of η_K, which reads

$$\lambda_{K,1}\, \frac{\mathbf{u}_{K,1}^\top\, G_K^*(v)\, \mathbf{u}_{K,1}}{\mathbf{u}_{K,1}^\top\, \mathbf{u}_{K,1}}\,,$$

because of $|\mathbf{u}_{K,1}| = 1$. Since $\lambda_{K,1} \gg \lambda_{K,d}$ for anisotropic elements, the refinement process should try to minimize the quotient such that the whole term does not dominate the error over K. Obviously, we are dealing here with the Rayleigh quotient, which is minimal if $\mathbf{u}_{K,1}$ is the eigenvector to the smallest eigenvalue of $G_K^*(v)$. As consequence, the longest stretching of the polytopal element K should be aligned with the direction of this eigenvector. In order to achieve the correct alignment for the next refined mesh, we may bisect the polytopal element orthogonal

to the eigenvector which belongs to the largest eigenvalue of $G_K^*(v)$. Thus, we propose the following refinement strategies:

ISOTROPIC The elements are bisected as introduced in Sect. 2.2.3, i.e., they are split orthogonal to the eigenvector corresponding to the largest eigenvalue of $M_{\mathrm{Cov}}(K)$.

ANISOTROPIC In order to respect the anisotropic nature of v, we split the elements orthogonal to the eigenvector corresponding to the largest eigenvalue of $G_K^*(v)$.

Both refinement strategies do not guaranty the regularity of the meshes since there is no control on the edge lengths due to the naive bisection. This might be imposed additionally in the realization, but the approach also works well in the forthcoming tests without this extra control.

For the numerical experiments we consider $\Omega = (0, 1)^2$ and the function

$$v(x_1, x_2) = \tanh(60x_2) - \tanh(60(x_1 - x_2) - 30) \,, \tag{3.18}$$

taken from [109], which has two sharp layers: one along the x_1-axis and one along the line given by $x_2 = x_1 - 1/2$. The function as well as the initial mesh is depicted in Fig. 3.5. We apply the BEM-based FEM as usual, although the local BEM solver is not tailored for the anisotropic elements. For the details on the realization see Chap. 4.

Test 1: Mesh Refinement

In the first test we generate several sequences of polygonal meshes starting from an initial grid, see Fig. 3.5 right. These meshes contain naturally hanging nodes and their element shapes are quite general. First, the initial mesh is refined uniformly,

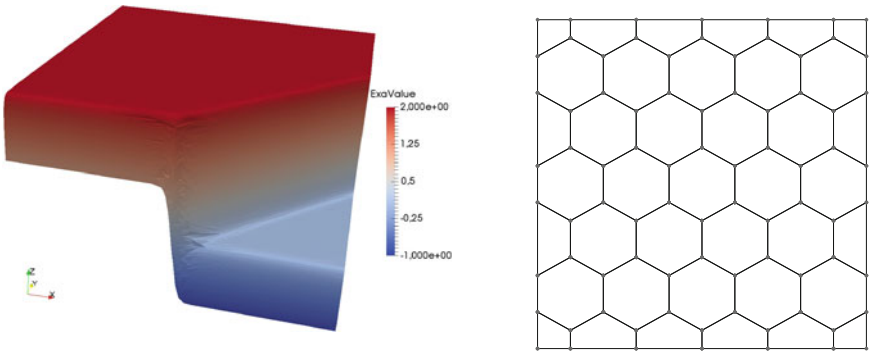

Fig. 3.5 Visualization of function with anisotropic behaviour (left) and initial mesh (right)

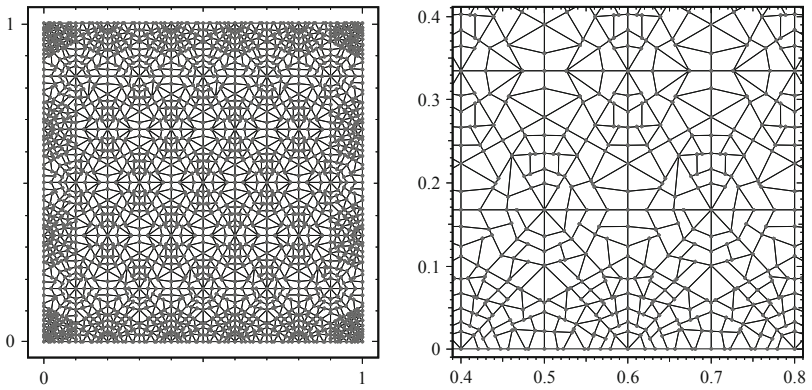

Fig. 3.6 Mesh after six uniform refinement steps using the ISOTROPIC strategy and zoom-in

i.e., all elements of the discretization are bisected in each refinement step. Here, the ISOTROPIC strategy is performed for the bisection. The mesh after six refinements as well as a zoom-in is depicted in Fig. 3.6. The uniform refinement clearly generates a lot of elements in regions where the function (3.18) is flat and where only a few elements would be sufficient for the approximation.

Next, we perform the adaptive refinement algorithm as described above for the different bisection strategies. The generated meshes after 6 refinement steps are visualized in Figs. 3.7 and 3.8 together with a zoom-in of the region where the two layers of the function (3.18) meet. Both strategies detect the layers and adapt the refinement to the underlying function. The adaptive strategies clearly outperform the uniform refinement with respect to the number of nodes which are needed to resolve the layers. Whereas the ISOTROPIC strategy in Fig. 3.7 keeps the aspect ratio of the polygonal elements bounded, the ANISOTROPIC bisection produces highly anisotropic elements, see Fig. 3.8. These anisotropic elements coincide with the layers of the function very well.

Finally, we compare the error measure η for the different strategies. This value is given with respect to the number of degrees of freedom, which coincides with the number of nodes, in a double logarithmic plot in Fig. 3.9. The error measure decreases most rapidly for the ANISOTROPIC strategy and consequently these meshes are most appropriate for the approximation of the function (3.18). The convergence order for η has not been studied analytically, however, we observe faster decrease for the ANISOTROPIC refinement in this test for the considered range. This behaviour might result from a pre-asymptotic regime. A slope of $1/2$ for $d = 2$ corresponds to linear convergence in finite element analysis.

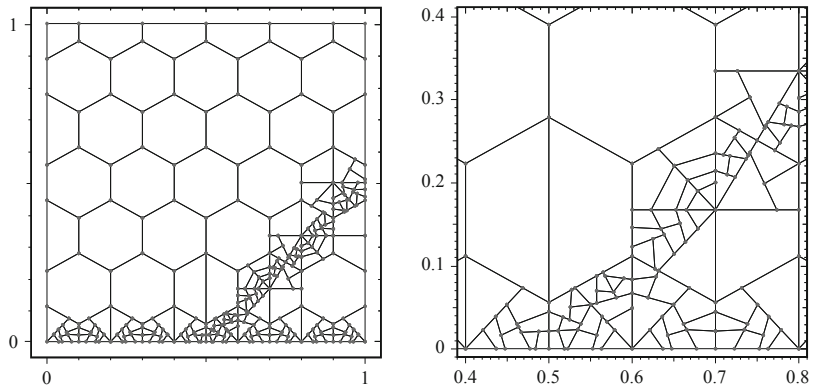

Fig. 3.7 Mesh after six adaptive refinement steps for the ISOTROPIC strategy and zoom-in

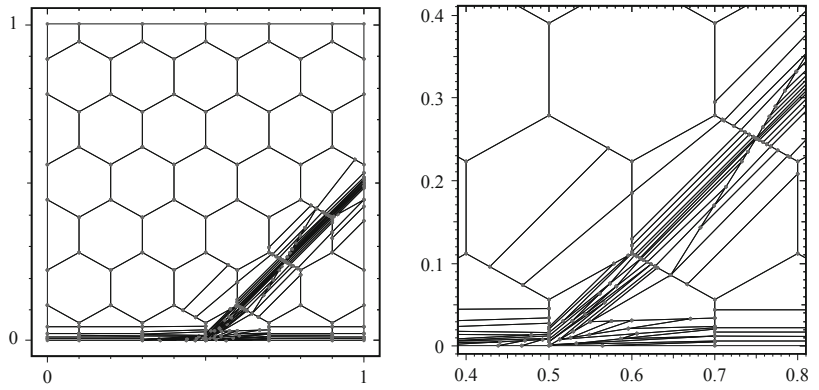

Fig. 3.8 Mesh after six adaptive refinement steps for the ANISOTROPIC strategy and zoom-in

Test 2: Mesh Properties

We analyse the meshes more carefully. For this purpose we pick the 13th mesh of the sequence generated with the ISOTROPIC and the ANISOTROPIC adaptive refinement strategy. In Sect. 3.4.1, we have introduced the ratio $\lambda_{K,1}/\lambda_{K,2}$ for the characterisation of the anisotropy of an element. In Fig. 3.10, we give this ratio with respect to the element ids for the two chosen meshes. For the ISOTROPIC refined mesh the ratio is clearly bounded by 10 and therefore the mesh consists of isotropic elements according to our characterisation. In the ANISOTROPIC refined mesh, however, the ratio varies in a large interval. The mesh consists of several isotropic elements, but there are mainly anisotropic polygons. The ratio of the most anisotropic elements exceeds 10^5 in this example.

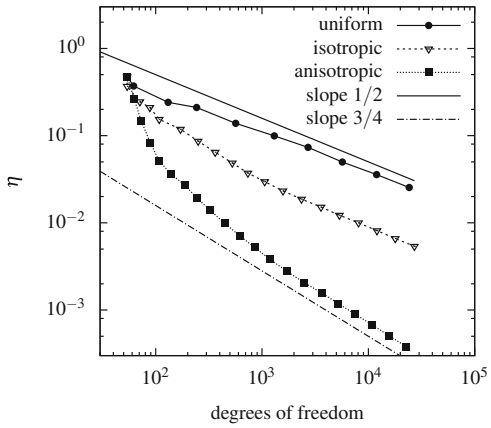

Fig. 3.9 Convergence graph of the anisotropic error measure η with respect to the number of degrees of freedom for the different refinement strategies

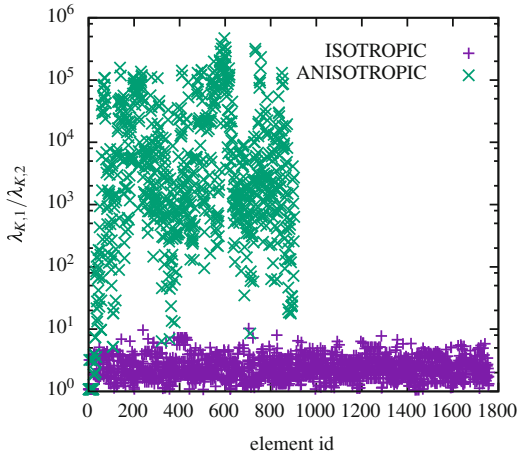

Fig. 3.10 Quotient $\lambda_{K,1}/\lambda_{K,2}$ for all elements in the 13th mesh of the sequence with ISOTROPIC and ANISOTROPIC adaptive refinement

Next we address the scaling parameter α_K in these meshes. In the comparison of the derived estimates with those of Formaggia and Perotto [79], it has been assumed that $\alpha_K \sim 1$. In Fig. 3.11, we present a histogram for the distribution of α_K in the two selected meshes. As expected the values stay bounded for the ISOTROPIC refined mesh. Furthermore, α_K stays in the same range for the ANISOTROPIC refinement. In our example, all values lie in the interval $(0.28, 0.32)$ although we are dealing with elements of quite different aspect ratios, cf. Fig. 3.10.

Test 3: Interpolation Error

In the final test we apply the pointwise interpolation into the space V_h to the function (3.18) over the meshes generated in this section. The convergence of the interpolation is studied numerically for the different sequences. We consider the interpolation error in the L_2-norm. In Fig. 3.12, we give $\|v - \mathfrak{I}_h v\|_{L_2(\Omega)}$ with respect to the number of degrees of freedom in a double logarithmic plot, where $\mathfrak{I}_h : H^2(\Omega) \to V_h$ is defined as in Sect. 2.4. Since $v \in H^2(\Omega)$ in this experiment,

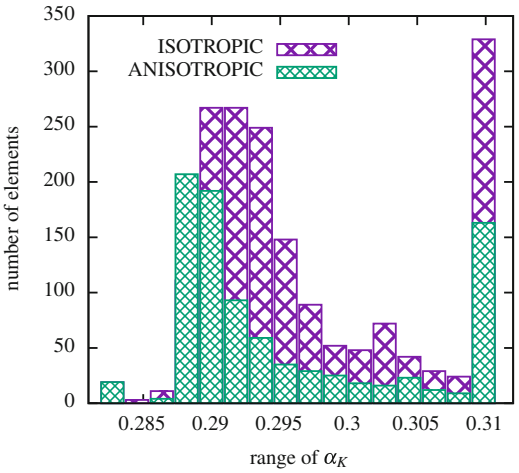

Fig. 3.11 Histogram for the distribution of α_K for the 13th mesh in the sequence with ISOTROPIC and ANISOTROPIC adaptive refinement

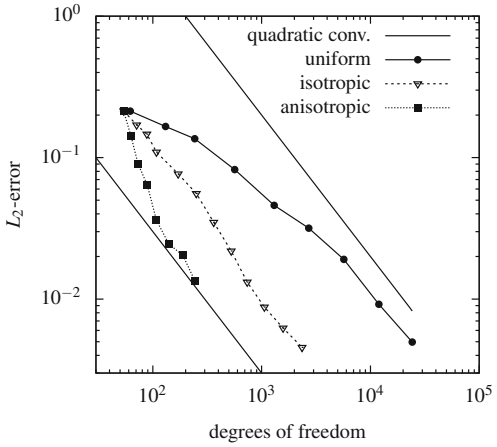

Fig. 3.12 Convergence graph of the L_2-error of pointwise interpolation with respect to the number of degrees of freedom for the different refinement strategies

we expect quadratic convergence with respect to the mesh size on the sequence of uniformly refined meshes. This convergence rate corresponds to a slope of one in the double logarithmic plot in two-dimensions. In Fig. 3.12, we observe that the uniform refinement reaches indeed quadratic convergence after a pre-asymptotic regime. The optimal rate of convergence is achieved as soon as the layers are resolved in the mesh. On the adaptively generated meshes, however, the interpolation error converges with optimal rates from the beginning. We can even recognize in Fig. 3.12 that the ANISOTROPIC refined meshes outperform the others. The layers are captured within a few refinement steps. Therefore, the error reduces faster than for the ISOTROPIC refined meshes before it reaches the optimal convergence rate.

Let us compare the seventh meshes in the sequences which are obtained after six refinements and which are visualized in Figs. 3.6, 3.7, and 3.8. For the uniformly refined mesh we have 2709 nodes and it is $\|v - \mathfrak{I}_h v\|_{L_2(\Omega)} \approx 3.17 \times 10^{-2}$. The adaptively refined mesh using ISOTROPIC bisection contains only 363 nodes but yields a comparable error $\|v - \mathfrak{I}_h v\|_{L_2(\Omega)} \approx 3.49 \times 10^{-2}$. The most accurate approximation is achieved on the ANISOTROPIC refined mesh with $\|v - \mathfrak{I}_h v\|_{L_2(\Omega)} \approx 2.04 \times 10^{-2}$ and only 189 nodes. A comparable interpolation error to the other refinement strategies is obtained on the fifth mesh of the sequence of ANISOTROPIC refined meshes. This mesh consists of 108 nodes only.